國立交通大學

照明與能源光電研究所

碩士論文

二氧化鈦奈米管陣列與複合結構在染料敏化太陽能電池之應用

Dye-Sensitized Solar Cell using TiO_2 Nanowires on Anodic TiO_2 nanotube Arrays (TNWs/TNAs)

研究生：楊雅婷

指導教授：呂志鵬 博士

中華民國一百零一年九月

二氧化鈦奈米管陣列與複合結構在染料敏化太陽能電池之應用

Dye-Sensitized Solar Cell using TiO_2 Nanowires on Anodic TiO_2 nanotube Arrays (TNWs/TNAs)

研究生：楊雅婷　Student：Ya-Ting Yang
指導教授：呂志鵬　教授　Advisor：Dr. Jihperng Leu
楊界雄　教授　Dr. Kei-Hsiung Yang

國立交通大學
照明與能源光電研究所
碩士論文

A Thesis
Submitted to Institute of Lighting and Energy Photonics
College of Photonics
National Chiao Tung University
in partial Fulfillment of the Requirements
for the Degree of
Master
in

Lighting and Energy Photonics

September 2012

Hsinchu, Taiwan, Republic of China

中華民國一百零一年九月

二氧化鈦奈米管陣列與複合結構在染料敏化太陽能電池之應用

研究生：楊雅婷　　　　　　　　　　指導教授：呂志鵬　博士

楊界雄　博士

國立交通大學

照明與能源光電研究所

摘要

染料敏化太陽能電池(Dye-sensitized solar cell, DSSC)是目前極具發展潛力的新一代有機太陽能電池。其中光電極表面形貌是影響效率的主因之一，期望利用二氧化鈦奈米管一維陣列結構改善電子傳輸而提升效率且未來發展可饒式元件具有較高的穩定性。

本論文中，含乙二醇,氟化銨及含水之電解液以陽極氧化處理法，於鈦板製備二氧化鈦奈米陣列(TNAs)及其複合結構(TNWs/TNAs)薄膜層上。實驗中由電壓、時間及攪拌對於結構變化關係可推論其形成機制並利用其變化製作相同厚度薄膜，但不同形貌之二氧化鈦光電極。進而探討不同電壓時間,產生不同結構 TNAs 及 TNWs/TNAs。進而應用於染料敏化太陽能電池光轉換效率影響。

由光電轉換效率及可見光光譜儀檢測在相同膜厚(12μm)，奈米線複合結構染料吸附量較僅奈米管結構來的多，透過提升吸附染料而提高光電流密度，而有較好的光電轉換效率。於 30 伏特電壓下製備 8 小時之二氧化鈦複合結構染料吸附相對純奈米管結構有 21%的差異且轉換效率達 $\eta=1.85\%$,其中電流密度由 3.80 提高至 5.27 (mA/cm^2) 。

Dye-Sensitized Solar Cell using TiO_2 Nanowires on Anodic TiO_2 Nanotube Arrays (TNWs/TNAs)

Student: Ya-Ting Yang
Advisor: Dr. Jihperng (Jim) Leu
Dr. Kei-Hsiung Yang

Institute of Lighting and Energy Photonics
College of Photonics
National Chiao Tung University

ABSTRACT

Dye-sensitized solar cell (DSSC), a new generation solar cell, has the potential to be widely used due to its advantages of low cost, compatibility for flexible devices, and enhanced performance with temperature. Specifically, the morphology of TiO_2 film is one of the major factors affecting the conversion efficiency. Among various structures, TiO_2 nanotube has great potential due to the highly ordered could provide a direct transport route and higher stability for flexible device.

In this study, a TNWs/TNAs hybrid structure was first fabricated using a one-step method by anodizing a titanium foil in electrolytes consisting of NH_4F and H_2O, under different voltage and processing time. The evolution and the mechanism of TNWs/TNAs hybrid structure prepared by using mechanical stirring were examined and proposed. The DSSC performance of TNWs/TNAs was measured and compared to TNAs and conventional TiO_2 nanoparticle film. Based on the I-V characteristics and dye absorption measurement by an UV-visible spectroscopy, nanowires in the TNWs/TNAs (12 μm) hybrid structure enhance the surface area and improve the redox couple diffusion in TiO_2 electrode to raise the photocurrent, resulting in enhanced conversion efficiency. For TNWs/TNAs hybrid structure (30V, 8 hours), the conversion efficiency and J_{sc} are 1.85%, 5.27 mA/cm^2, compared to 1.04% and 3.81 mA/cm^2 in a TNA only film. The 44.3% improvement in conversion efficiency can be attributed to the enhanced dye adsorption (21%) and better electron transport in TNWs/TNAs compared to TNAs only. Overall, TNWs/TNAs films show great potential to be a simple and flexible DSSC.

Acknowledgements

很榮幸能夠進入交大光電學院就讀碩士學位，在台南校區的時光雖不長卻與同伴有著深厚的情誼 。 感謝楊界雄老師在台南校區時的教學以及照顧，進入呂志鵬老師實驗室後，非常感謝老師在各實驗方向上的提點，且在論文內容上對我的引導跟指正。 在碩士期間，老師除了提供實驗上的支持，同時為增進實驗室成員們的情誼也舉辦了很多活動，讓這段研究所時光充滿了許多回憶。

每周的會議上，老師總會對於報告提出意見:教導應具備的邏輯思維、檢討實驗步驟及對實驗環境安全的提點。促使我們能夠更加細心及注意的檢視進而改進。

進入實驗室，非常感謝各位熱心的學長姊 。無論是實驗室事務的交接還是實驗上的承襲都受益良多 。 其中明義學長及幸鈴學姊是使我能夠畢業的最大功臣，實驗上的帶領以及面對問題時的解惑，學長姐們總是能夠給我一個很好的方向及答案。 一方面也教導我資料應該如何整理、文獻應該如何去研讀等等事情都能透過與各位學長姊的談話中，獲得了不少啟發。

同儕之間，維剛在我有需要幫助時，總是義不容辭的給予支援及意見，且總能夠在談話中獲得許多不同領域的知識。在丞芳的陪同下，我們總是歡樂的一同做著實驗，即使是面對挫折也能夠一同商討互相打氣。

龍哥、王智及大龜學長們的幽默常常讓整個實驗室氣氛活絡而弘恩學長總是不厭其煩的代為操作 FIBSEM，真的相當的感謝。 也感謝上一屆的學長:小胡 、阿爆、沁穎及書豪們的實驗經驗分享以及學妹麒雅在實驗上的支援與幫助。透過認識大家而增長見聞，一起度過了在交大的校園時光。

另外要感謝軍華實驗室的政衡， 因為有你的幫助實驗才能夠順利的進行 。而好友炫文及冠名總在我失落或是熬夜時刻，以簡訊打電話的方式不斷提醒要我保重身體。 不斷鼓勵我和聽我抱怨，真的非常的感動能有這樣的摯友。

最後，我要由衷感謝我的家人讓我在這樣無憂無慮的環境下，一路學習至今並且總是支持我的決定及想法，感謝你們的付出及陪伴。

Contents

Table Captions

Figure Captions

Chapter 1 Introduction

After industrial revolution, energy consumption increased drastically. Since 19th century, new kind of energy, especially fossil fuel, was developed one after another. However, the reserves of petroleum are limited and going to be exhausted by this century. Also, the widespread usage of fossil fuel has caused serious environmental pollution and ecological damage. United Nation Framework Convention on Climate Change (UNFCCC) and Kyoto Protocol clearly emphasize the importance of renewable energy development.

Renewable energy including waterpower, wind power, solar, biologic energy, and terrestrial heat, can transfer into electric power, heat, chemical power and fuel. In all kinds of energy, solar energy is almost inexhaustible and without environment pollution. The supply of energy from the Sun to the Earth is gigantic: 3×10^{24} joules a year, or about 10,000 times more than the global population currently consumes, which means converting 0.1% of the Earth's surface using solar cells with an efficiency of 10% would theoretically satisfy our present needs. [1]

Nevertheless, the solar energy from the sun cannot be use efficiently. Part of the sun power would be absorbed by the Earth's atmosphere or reflected to space. Even though the sun energy is hard to be used efficiently, solar power still offers a realistic solution to energy problems. This is the reason why solar cells have attracted extensive attention and fast development. . Solar can be transformed to electricity, fuels, and heat passes without noise. And it produces no air pollution. Massive solar power conversion would ensure abundant energy and safe clear environment for future generations. In all kinds of solar cells, silicon (Si) based solar cells are more mature to become the main products on the market. However, the cost of silicon base solar cells is relatively high.

Therefore, it is important to develop solar cells with low cost and high conversion efficiency for popular use.

B. O’Regan and M. Grätzel in 1991 developed a new kind of solar cell, dye-sensitized solar cell, which has relatively high conversion efficiency, simple fabrication process, low production cost, and transparency [2]. In 2011, great conversion efficiency 12.3 % has been reported for DSSC based on nanocrystalline TiO2 film, ruthenium sensitized dye, triiodide/iodide redox couple in organic solvent as the electrolyte and platinum coated counter electrode. [3]

The performance and efficiency of the DSSC depend on many factors such as the platinum layer of the counter electrode, the TiO_2 layer surface morphology and the structure, dye molecules, the status and component of the electrolyte. In the TiO_2 layer, mesoporous nanocrystalline TiO_2 films provide large surface area for dye adsorption, electrical connection with the redox electrolyte, electron diffusion and transportation. However, the efficiency was limited at interface traps and electrons recombination. In recent years, various forms of TiO_2 nanostructures such as nanorods, nanotubes, and nanowires have attracted significant research interests to enhance the electron transportation [4,5]. Several studies reported that one dimensional TiO_2 nanostructure could improve the charge-collection efficiency by promoting a better transport route than nanoparticles. [6,7,8] and resulted in lowering electron-hole recombination probability [9].

TiO_2 nanotube arrays (TNAs) grown by electrochemical anodization method was first reported by Zwilling et al. [69] with a length up to 500 nm (10:1 aspect ratio) using HF-based aqueous electrolyte. Several neutral electrolytes such as ethylene glycol (EG) or ammonium fluoride (NH_4F), have been employed to prepare anodized TiO_2 nanotubes with a higher aspect ratio [74,75]. Specifically, high aspect ratio (100:1), self-organized TiO_2 nanotubes have been produced using EG solution [73]. However, most of studies have been dedicated to one specific type of 1D TiO_2 structures such as nanotubes, nanorods, or nanowires, with less research on 1D TiO_2 hybrid structures. Lim and Choi [10] demonstrated the TiO_2 nanowires directly connected TiO_2 nanotubes arrays structure (designated as TNWs/TNAs) using EG and NH_4F under mechanical stirring and proposed a bamboo-splitting model. Recently, Hsu et al. [100] fabricated TNWs/TNAs hybrid structure by a one-step anodization method without mechanical stirring, for photocatalysis application. Yet, little work has been reported on the applications of TNWs/TNAs and TNAs for DSSC, especially as a flexible device. Also, the details of the formation mechanism for TNWs/TNAs under stirring still needs to be clarified.

This study investigates a one-step method for the fabrication of a TNWs-covered TNAs (TNWs/TNAs) hybrid structure, using a mixture of EG and water containing NH_4F electrolyte with and without mechanical stirring. The morphology of the TNWs/TNAs structure was then examined by changing the anodizing voltage and processing time, to elucidate the detailed formation mechanism of TNWs/TNAs. The DSSC performance of TNWs/TNAs and TNAs structures was investigated and compared with the film made of TiO_2 nanoparticles.

1.2 Overview

This thesis is organized in five Chapters. In Chapter 1, the advantages and working principle of dye-sensitized solar cells (DSSCs) are introduced. One-dimensional TiO_2 structures including TiO_2 nanotubes (TNAs) and TiO_2 nanowires/TNAs hybrid structure for photocatalysis and DSSC applications have been used for photocatalysis application. In this study, the preparation of TNWs/TNAs hybrid structures was examined at various applied voltage and time under stirring, compared those prepared without mechanical stirring of solution. Also, we plan to further explore the TNWs/TNAs hybrid structure for DSSCs application.

Chapter 2 reviews the literatures of the anodizing oxidation method for preparing TNAs and TNWs/TNAs hybrid structure. Chapter 3 covers the experimental details of preparing TNWs/TNAs hybrid structure and the electric measurement of DSSC performance. In Chapter 4, we focus on the results and discussion on the fabrication and formation mechanism of TNWs/TNA hybrid structure using mechanical stirring of solution. In addition, the performance of DSSC based on TNWs/TNA hybrid structure was illustrated and compared to DSSCs based on TiO_2 particles, TNAs, and TNWs/TNAs. At last, summarize the key findings and contribution of this work as well as the future work in Chapter 5.

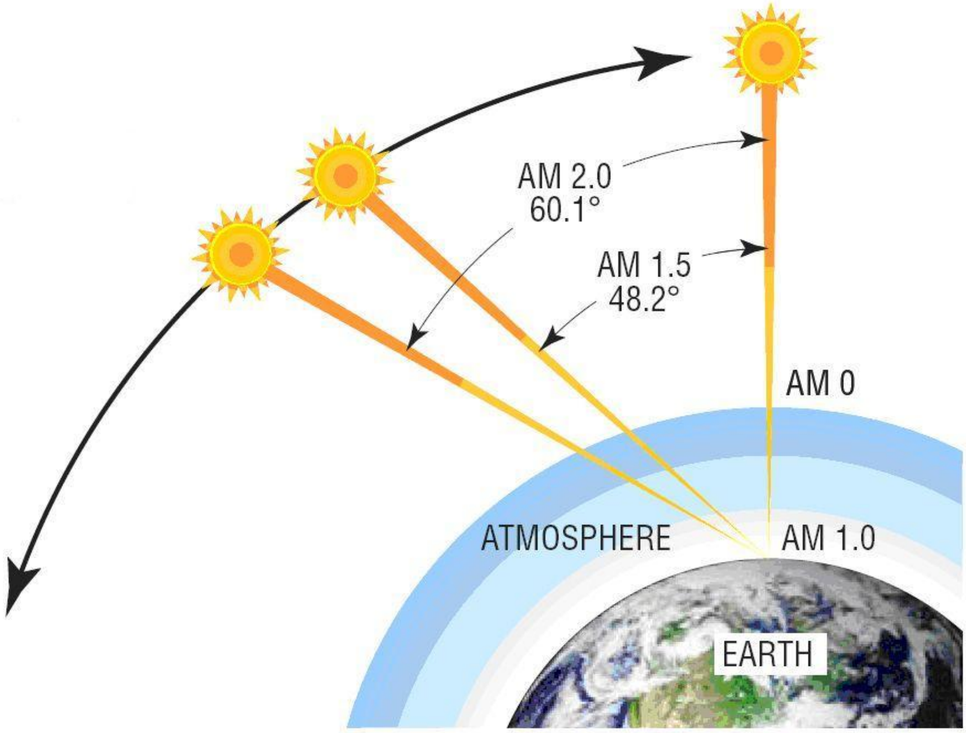

Figure 1.1 The path length, in units of Air Mass, changes with zenith angle. [11]

Chapter 2 Literature Review

2.1 Dye-sensitized Solar Cell

In 1991 Brian O'Regan and Michael Grätzel proposed a high efficiency photovoltaic cell with TiO_2-based film as semiconductor electrode, ruthenium (Ru) organometallic compound as light sensitizer, and suitable redox couple solution as electrolyte [4]. This solar cell called "dye-sensitized solar cell" which had 7.1% conversion efficiency under sun illumination. The cell conversion efficiency reached a breakthrough, 10% in 1999 [12]. The best record (2011) of DSSC conversion efficiency is higher than 12.3%, using porphyrin as a sensitized dye, and Cobalt (II/III) as redox electrolyte. [13]

2.1.1 The Structure and Working Principle of DSSC [1]

The structure of DSSC is a sandwich structure consisting of TCO glass, dye sensitized TiO_2 layer, electrolyte, and platinum coated counter electrode.

Figure 2.1 demonstrates the schematic structure of DSSC. The photoanode, which is made of TiO_2 dye-sensitized semiconductor, receives electrons from the photo-excited dye which is oxidized. The oxidized dye molecules then turn to oxidize the mediator, the redox species in the electrolyte and regenerate dye. The mediator is regenerated by the redaction at the cathode by the electrons circulated through the external.

1. Photoexcitation on dye molecules to induce charge separation:

$$Dye + h\nu \rightarrow Dye^{*} \qquad (2\text{-}1)$$

2. Charge (electron) injects into conduction band of TiO_2:

$$Dye^{*} \rightarrow Dye^{+} + e^{-}_{TiO_2} \qquad (2\text{-}2)$$

3. Charge passes through outer circuit via electronic load:

$$e^{-}_{TiO_2} \longrightarrow e^{-}_{counter} \qquad (2\text{-}3)$$

4. Dye reduces to ground state by redox couple in the electrolyte:

$$2Dye^{+} + 3I^{-} \rightarrow 2Dye + I_3^{-} \qquad (2\text{-}4)$$

5. Redox couple reduces on counter electrode by the charge comes from outlet circuit:

$$I_3^{-} + 2e^{-}_{counter} \rightarrow 3I^{-} \qquad (2\text{-}5)$$

The Total Reaction:

$$e^{-}(counter) + hv \rightarrow e^{-}(TiO_2\ electrode) \qquad (2\text{-}6)$$

The TiO_2 electrode does not work as the main light absorption character, but used a carrier transport host material inside DSSC systems. The synthesized organic dye attached to TiO_2 absorbs almost the visible light and made carrier injected from excited dye molecules then quickly transport to the current collector and then the outer circuit. It avoids the direct charge recombination, which is the energy-favored process after charge separation. The electrons and holes run different routes back to their ground state; this important property contributes to the unusual charge separation efficiency inside DSSC systems.

The root-causes for low DSSC conversion efficiency include, for example, electron/hole recombination inside DSSC, resistance of the materials and impedance at each material interface. The main recombination reactions are at TiO_2/dye interface and TiO_2/electrolyte interface, which might cause photocurrent loss.

Equation of recombination at TiO_2/dye interface:

$$Dye^{+} + e^{-}_{TiO_2} \rightarrow Dye \qquad (2\text{-}7)$$

Equation of recombination at TiO_2/electrolyte interface:

$$3I^{-} + 2e^{-}_{TiO_2} \rightarrow I_3^{-} \qquad (2\text{-}8)$$

The resistance is decided when the material was chosen, but the impedance at each interface can be reduced by surface modification and post-treatment to improve the connection of each materials.

2.1.2 Operation Principles of Dye-sensitized Solar Cells

1. Open Current Voltage (V_{OC}) Characteristics

When photovoltaic devices are under illumination, the open circuit voltage can be calculated from the diode equation. [14]

$$V_{OC} = \frac{nRT}{F} \, ln \left(\frac{i_{sc}}{i_0} - 1 \right) \qquad (2\text{-}9)$$

Where n is the ideality factor whose value is between 1and 2 for DSSC, and i_0 is the reverse saturation current, which can be measured in reasonably large reverse voltage. There are two main characteristic quantities, the open circuit voltage (V_{OC}), which represents the voltage produce in the absence of any current, and short circuit current (I_{SC}), which stands for the current with no voltage across the cell.

The open circuit voltage is determined by the energy difference between the Fermi level of the semiconductor under illumination and the Nernst potential of the redox couple in the electrolyte. However, the experimentally observed open circuit voltage for various sensitizers is smaller than the difference between the conduction band edge and the redox couple. This is generally due to the competition between electron transfer and charge recombination. [15]

When photovoltaic devices are in dark, they should obey the ideal diode equation:

$$I = I_{sc}\left(e^{qV/kT} - 1\right) \qquad (2\text{-}10)$$

This indicates that a positive applied voltage can make current flow easy.

2. Incident Photons to Current Conversion Efficiency (IPCE)

IPCE is an important parameter when determining the performance of a photovoltaic device. IPCE is defined as the number of electrons flowing through the external circuit over the number of photons incident on the cell surface at a particular wavelength, which means IPCE the ratio of the observed photocurrent over the incident photon flux.

3. Cell Efficiency (η)

We called V_{OC} as the maximum voltage at photovoltaic device, and I_{SC} as the maximum short circuit current under illumination. The IV-curve yielding the maximum power is called P_{MAX}. In addition, another important parameter of cell performance is the Fill Factor (FF), which is defined as follows:

$$FF = \frac{P_{MAX}}{V_{OC} \times I_{SC}} \tag{2-11}$$

FF is an efficiency factor, used for checking whether the P_{MAX} is ideally equal to $V_{OC} \times I_{SC}$ or not, because there are many types of impedances, including the contact resistance, electrolyte resistance, and charge transfer resistance, etc. inside the cell, may cause potential drop.

The overall energy conversion efficiency (η) is defined to be the maximum power generated by DSSC under illumination:

$$\eta_{eff} = \frac{P_{MAX}}{P_{ill}} \times 100\% = \frac{V_{OC} \times I_{SC} \times FF}{P_{ill}} \times 100\% \tag{2-12}$$

Equation *(2-10)* indicates high open circuit voltage and short circuit current are necessary for high overall efficiency, but the conversion efficiency will still be low without high fill factor (FF).

2.2 Components of DSSCs

2.2.1 Substrate

The most commonly used substrates for DSSC are transparent conducting oxide (TOC) coated glass substrates. For meeting the trend of consumer electronic devices, a new focus of DSSC technology is directed to the realization of light weight film-type cells. Electrochemical anodic oxidization of titanium metal foil could fabricate highly ordered TiO_2 array. Therefore, TCO coated solid glass substrate is replaced with a TiO2 nanotube arrays and TiO_2 nanowires/TNA hybrid on a Ti foil in this study.

2.2.2 Nanocrystalline Photo-anode

Titanium dioxide is a fundamental semiconductor for DSSC because of its non-toxic properties, easy produce process, high stability and low cost. Energy conversion in a DSSC is based on the injection of an electron from a photo-excited state of the sensitizer dye into the conduction band of semiconductor.

For nanoparticle TiO_2 film, there are two methods to prepare photoanode. One is the “sol-gel method” [16,17], by which TiO_2 is prepared from hydrolysis of Ti-alkoxides and addition of a binder. Narrow particle size distribution and fine-ordered crystal structure can be obtained by carefully controlling every preparing step. However, this method is limited to small scale for laboratory only, although these properties are desired in standard electrode.

Nanoparticle efficiency was limited in the random walking of electron transport and recombination. To improve the efficiency of charge collection and reduce the recombination, different TiO_2 morphologies, such as vertically TiO_2 nanotube arrays, nanorods, and nanowires, have been investigated. Recently, TiO_2 nanotubes were applied in solar cells. [1] The conversion efficiency was reported to increase from 1.6% to 1.9% under various tube length and morphology. [1]

There are many methods for preparing nanostructured TiO_2 electrodes, including electrodeposition [18,19,20], evaporation[21], sputter deposition [22,23,24,25,26], and chemical vapor deposition [27,28]. The highly-ordered TiO_2 nanotube arrays [29] and mixture of TiO_2 nanowires and nanoparticles [30] are typically used as the photo-electrode.

The formation mechanism of TiO_2 nanotube arrays (TNAs) and mixture of TiO_2 nanowires (TNWs/TNAs) structures are similar to anodic aluminum oxide (AAO), which is the result of competition between field-assisted anodic oxidation and electrochemical etching. “Electrochemical anodization method” which Zwilling and co-worker published the first report on anodized TiO_2 nanotube in 1999. [11] The typical porous structure observed only in sufficient HF was added to the electrolyte mixture called the first generation. In subsequent work, the smooth and long tube has been controlled in various electrolytes due to the different ion diffusion and the amount of water. [31,32]

2.2.3 The Sensitizer: Organic dye

As mentioned before, the organic dye becomes a sensitizer which absorbs most of the incident light and increases the cell efficiency. Organic dye used in photoelectron chemical cells should meet the follow needs:

1. Absorption: With good absorption in visible light region up to wavelength 920nm, almost the incident light from sun.

2. Energetic: With sufficient electrons on excited state providing the driving force to make electrons inject to conduction band of TiO_2 thin film. Organic dye should also have relative low ground state for reduction by the redox couple in electrolyte.

3. Kinetics: The rate of electron injection should be high, and the lifetime of excited electrons should be long enough.

4. Stability: The organic dye can be operated under normal environment for more than 10^8 times of the redox cycle reaction and can be operated for more than 20 years.

5. Interfacial properties: It can attach on TiO_2 surface and cannot be easily desorbed from TIO_2 electrode.

A breakthrough of organic sensitized dye is accomplished by Grätzel’s group at EPFL in Switzerland by using metallo-organic ruthenium complex as the “dye” along with nanostructured TiO_2 electrode.[4] The dye have the general structure $ML_2(X)_2$, where L stands for 2,2’-bipyridyl-4,4’-dicarboxylic acid, M for ruthenium or osmium and X for halide, cyanide, thiocyanate. The cis-RuL_2 $(NSC)_2$, also called N3 dye has shown impressive performance. Figure 2.2 compares the spectral response of the photocurrent observed with two sensitizers. The incident photo to current conversion efficiency (IPCE) of DSSC is plotted as a function of excitation wavelength. Both chromophores show high IPCE values in the visible range. However, the response of the black dye extends 100nm further into the IR than of N_3. The photocurrent onset is close to 920 nm, i.e. near the optimal threshold for single junction converters. Recently, there is a credible challenger identified to the “black dye” (tri(isothiocyanate)-2,2’,2”-terpyridyl-4,4’4” -tricarboxylate)Ru (Ⅱ).

Lately several studies showed up by modifying the function groups to improve excitation lifetime and increase the open circuit voltage of the cell which are called N719, N749 (black dye)…etc. (see Figure 2.3).

Recent work has focused on the molecular engineering of suitable ruthenium compounds, which are known for their excellent stability. Cis-Di-(thiocyanato)bis(2,2’-bipyridyl-4,4’-dicarboxylate)ruthenium(Ⅱ), coded as N3 or N719 dye depending on whether it contains four or two protons. N719 dye was found to be an outstanding solar light absorber and charge-transfer sensitizer. Figure 2.4 shows the structures of three ruthenium complexes with different colors that have been widely employed as sensitizers for the DSSC. This feature can be applied to design multicolor DSSC in art and architecture.

Another important issue being raised up lately is the dye adsorption process, in which the sintered TiO_2 electrode is immersed into a dye solution, usually 2×10^{-4}M in solvent traditionally. The dye adsorption should be done immediately after high temperature sintering process for TiO_2 electrode for not letting water content in the pores of electrode react with the excited dye molecules to reduce any impact on the long-term stability. In practice, we keep the photoelectrode in anhydrous condition before and after dye adsorption. The overall dye adsorption process should be stored in a moisture-free environment.

2.2-4 Electrolyte

Electrolyte systems consist of redox couple and solvent, which works as reducing agent providing electrons to redox the oxidized dye molecules at photoelectrode and as oxidant receiving from counter electrode.

Redox Couples

Requirements and properties of redox couple in electrolyte should be defined:

1. Redox potential

   The redox couple reversible potential has to be equal to the negative of dye reversible potential. The more negative the potential, the large the thermodynamic driving force for the dye regeneration. However the potential request should make the balance between the driving and the open circuit potential hence the cell performance in order to avoid unnecessary loss of usable energy.

2. High solubility

   To make sure sufficient supply of the redox mediator and to minimize the possibility of diffusion-limited situations, an adequate concentration of redox couple is needed. Because diffusion-limited would result in an undesirable lifetime of the oxidized dye and consequently would increase the possibility of dye decomposition. Concentration are commonly used at 0.1-0.5M

3. High diffusion coefficient

A high diffusion coefficient is needed because the mass transport of the redox couple in a solar cell (through solution and TiO_2 network) occurs solely by diffusion.

4. No significant spectral characteristics in the visible region. In order to prevent the situation of less light being available for the light-to-electricity conversion and thus low energy conversion, the redox couples should not able to have absorbance in the visible light region.

5. High stability of both the reduced and oxidized forms of couple

For efficient redox "shuttling" in solar cells, both the oxidized and reduced forms of the couple need to be present in solution and both forms must have high stability. In the case of iodide/triiodide system, the reduce form is in excess. [33,34]

6. Highly reversible couple

The oxidation of the reduce form and reduction of the oxidized form of the redox couple must be electrochemically and chemically reversible to ensure the fast electron transfer and avoid unwanted side reactions.

7. Chemically inert system

The components of the redox couple system must be chemically inert to avoid the side reaction, e.g., no chemical reactivity with TiO_2, no surface activity, etc. Based on the requirements listed above, many redox couples have been tested for DSSC systems. Now the I^-/I_3^- redox couple still remains the best choice because of its kinetics and suitable redox potential for TiO_2 electrode. In practical use, the redox couple is prepared by dissolving I_2 and some iodine salt such as KI, LiI, alkyl methylmidazolium iodide, etc. to form I^-/I_3^- couple. The triiodide would form instantaneously when iodide is added into iodide via this equation:

$$I^- + I_2 \rightarrow I_3^- \qquad (2\text{-}13)$$

Ionic liquid utilizing iodide as anion like DMPII (diemethyl-propyldazium iodide) has also been introduced to be iodide source in DSSC systems. It is believed that those “liquid-like” salts have higher dissociation rate than tradition iodide salt.

Solvents used for electrolyte

Some criteria are made for a suitable solvent for liquid-type electrolytes as below:

1. The solvents must be liquid and have low volatility at the operation temperature (usually 40-80℃) to avoid freezing or expansion of the electrolyte which would damage the whole cells.
2. They have low viscosity for rapid diffusion of carriers.
3. The chosen redox couple should have high dielectric constant to promote dissolution in solvent.
4. The solvent should not make desorption or dissolution of sensitized dye.
5. The solvent should not decompose under illumination or after long time use.
6. The solvent should better be low cost for large scale production, and have low toxicity.

Typical liquid solvents are acetonitrile (ACN) [35], methoxyactonitrile, methoxypropionitrile (MPN), ethylene carbonate (EC) [36], propylene carbonate [37], etc. and their mixture [38,39,40,41]. ACN has performed the best among these solvents, but it is still not well-received due to two reasons: (1) highly volatile with low boiling point (82℃) and (2) it is carcinogenic.

There are also new conceptions for the electrolyte of DSSC: Quasi-solid state polymer electrolyte, using ionic liquid as solvent for electrolytes containing an I^-/I_3^- redox couple. [42] The request for long-operation stability of DSSC is a driving force of to substitute liquid electrolyte by solid or quasi-solid state electrolyte. [43,44,45,46,47] However, the mass transport of the triiodide ion has been considered as a limiting factor for ionic liquids due to their low diffusion coefficient and lower concentration in these electrolytes versus iodide. A high concentration of redox couple is needed to achieve a domination of the exchange-reaction based fast charge transport process between I^- and I_3^- in viscous electrolytes. On the other hand, the absorption in visible light by I^- competes with the absorption of the dye and high concentration of I^- promotes the back electron transfer from conduction band of the photoanode to the triiodide [48].

2.2.5 Counter electrode

The reaction on counter electrode is a triiodide reduction:

$$I_3^- + 2e^- \rightarrow I^- \qquad (2\text{-}14)$$

This reaction plays an important role in the overall DSSC system because it is responsible for the regeneration of oxidized dye molecules. The conversion efficiency of DSSC might be lowered if the speed of dye regeneration is lower than the dye oxidization by photo injection.

Since the ITO or FTO shows slow kinetics of triiodide reduction in organic solvents [49,50], catalytic material is coated in order to accelerate the reduction reaction. Platinum (Pt) has been almost exclusively as the catalytic material. However, different methods preparing thin Pt film lead to different efficiency and cost. Fang *et al.* used sputtered Pt layer and they found out that the sputtered Pt layers on different type of substrates (steel sheet, nickel sheet, polyester film, and conducting plastic film) have slightly different cell efficiencies in comparison with that based on a conducting glass. [51] In recent reports, Kim *et al.* [52] have demonstrated the preparation of a new counter electrode consisting of Pt nanosized phase in NiO or TiO_2 porous phase using a RF co-sputtering system. They indicated that by applying Pt in a metal oxide biphase electrode, the short circuit current density and cell efficiency were increased due to the increased active surface area of the nanosized Pt.

Nonetheless, sputtering system is not proper for mass production considering the cost and the environment request of ultra-high vacuum. N. Papageorgiou [53] developed a method called “thermal cluster platinum catalyst” (TCP). Counter electrode made by this method has low Pt loading (around 2-10g/cm^3), superior kinetic performance, and mechanical stability comparing with other deposition methods like sputtering, spin coating, thermal [5, 54], and electrochemical deposition.

Wei *et al*. [55,56] developed a simple technique called “two-step dip coating” for preparing a Pt nanoclusters counter electrode for DSSC system. With an appropriate surface conditioner, the adhesion of PVP-capped Pt nanoclusters on ITO glass becomes satisfactory. Electrodes employing this method exhibit not only ultralow Pt usage but also good catalytic performance.

Other materials can be used as the counter electrode, such as conducting polymer [57,58], nanocarbon [59], carbon black [60,61] and carbon nanotubes [62]. Some even use polymer-catalyst composites [63,64,65]. These new material used as counter electrode usually requires porous film on the substrate to obtain acceptable catalytic reduction efficiency.

2.2.6 Sealant and Spacer

Sealing is a very important process in DSSC system to avoid the humid environment and to prevent the decomposition of dye molecules. The thickness of spacer is also having dilemma between making lower IR drop and the risk of short circuit.

Surlyn® (SX1170-60), a thermoplastic resin which has good toughness, becomes a good sealant used in DSSC. It is inert to electrolyte and shows great tightness. However, there are still other types of resin which also used in DSSC system.

2.2.7 Post-treatment/Pretreatments/Underlayer

Recent paper [66] revealed that a post-treatment of the TiO_2 film can efficiently improve the performance of DSSC based on the fact that an extra layer of TiO_2 is grown onto the TiO_2 nanotube arrays and hybrid nanowire structure constituting the film. There are many hypotheses concerning the following aspects:

(1) Surface area[67]

(2) Electron transport[64]

(3) TiO_2 purity[68]

(4) Dye anchoring[69]

These post-treatments have been carried out by $TiCl_3$ electrodeposition, Ti-isopropoxide and, the best, titanium tetrachloride ($TiCl_4$) post-treatment [70]. The effect of these post-treatment is believed to increase the dye loading making more efficient photon-current conversion which affect the short circuit current density (J_{SC}), and the current conversion efficiency (IPCE). It is also important to note that the $TiCl_4$ treatment would not be beneficial if a given TiO_2 nanoparticle film is already at the correct potential to reach the maximum efficiency of the electron injection, which depends on the history and source of TiO_2 to be made. In addition, another report indicates that the $TiCl_4$ pretreatment to ITO or FTO can certainly enhances the suppression of dark current leading an increase in V_{OC} and enlarge the surface area of the mesoscopic film leading the improvement of J_{SC} [71].

Xia *et al*. reported a new FTO/ TiO_X/ mesoscopic TiO_2 electrode was used as the blocking layer of DSSC [72]. According to their study, the blocking layer reduced the electron loss at the FTO/ mesoscopic TiO_2 and FTO/electrolyte interface by a TiO_2 compact layer between the FTO and mesoscopic TiO_2 layer which made by RF sputtering system. This is also another discovery finding out a layer made by TiO_2 can improve the total performance of DSSC due to various functions.

2.3 Anodic oxidization technique

2.3.1 The development of anodized TiO_2 nanotubes

First generation of TiO_2 nanotube

In 1999, Zwilling and co-workers anodizes Ti and Ti-6Al-4V (TA6V) alloy in an electrolyte containing 0.5 M chromic acid and 0.095 M HF [73], while the first report on anodized TiO_2 nanotubes (called first generation). The nanoporous structure observed only under a sufficiency HF was added to the electrolyte mixture, as pure chromic acid (CA) was leading to the formation of a thin but stable oxide layer with no apparent pore structure. Otherwise, the length of this kind method could enhance for a long processing time. TiO_2 nanotubes reach a steady state length when anodized. After typically 10 to 20 minutes of anodization, the etching rate equals the dissolution rate and it causes the length of nanotube stop increasing with additional anodizing time.

Second generation of TiO_2 nanotubes

Grimes and co-workers **[74]**overcome the limitation described before since they knew other fluorine salts (as fluorine ion source besides HF) and combined buffers, bases and milder acids to adjust the pH and fluorine ion content. Salts like KF, NH_4F, or NaF totally dissociate in aqueous solution and then hydrolyze with water to form HF [75]. Moreover, HF is a relatively mild acid in acidic solution ($pH<3.45$) more than 50% of the fluorine exist in the form of HF. As a result pH and fluorine ion concentration are closely related (and solutions with KF, NaF, and NH_4F and no additional acid are basic.) The experiments found that they could grow nanotubes up to 4.4 µm (Figure 2.5) using a solution of 0.1 M KF as fluorine source, 1 M H_2SO_4 as acid, 0.2 M citric acid presumably serving as buffer and NaOH as base to be added until the desired pH of 4.5 was obtained [72]. Later in 2005, Grimes and co-workers reported even longer nanotubes of up to 6 µm, over 17 to 20 h of anodization using the electrolyte as before [76].

Third generation of TiO_2 nanotubes

The third generation of nanotubes refer to smooth tubes (no ripples along the wall), prepared by using organic electrolytes (some almost water-free) to minimize the dissolution rate of formed oxides.

As illustrated in Figure 2.6 [77], it can be observed that tubes obtained in water are much rougher and irregular than the other. The reason was to use a viscous electrolyte, where ion diffusion is slower than in water. Meanwhile, the pH gradient between the bottom and top of the tubes increased. This led to the formation of TiO_2 nanotubes up to 7 μm thick (compared with the first generation). It implied that smoothness and regular morphology of the tube walls to the lower diffusion coefficient of the electrolyte which suppresses pH burst at the pore bottom which occur when working in aqueous media. TiO_2 nanotube arrays with lengths of up to 1000 μm were achieved using a non-aqueous, polar organic electrolyte such as formamide, dimethyl sulfoxide, ethylene glycol or diethylene glycol [78,79,80].

In 2007, Grimes and co-workers published the synthesis of 0.36 mm long nanotube [76], practically demonstrating that the nanotube lengths was only limited by the initial titanium foil thickness. The following section will discuss the fundamental aspects and chemistry of the growth of TiO_2 by anodization.

2.3.2 The growth of TiO_2 nanotube: fundamental aspects

The formation mechanism of TNAs nanostructure is similar to anodic aluminum oxide (AAO), which is the result of competition between field-assisted anodic oxidation, defined as the formation of the anodic layer under a applied electric field by Eq.(2-15)-(2-17) and chemical/field assisted dissolution of the forming oxide by Eq. (2-18), which can be regarded as dissolution promoted by the presence of fluoride ions (chemical dissolution) and by the electric field weakening the bond between Ti and O (field assisted dissolution)[81]:

Electrochemical reactions of anodic titanium oxide

At Ti / Ti oxide interface:

$Ti \rightarrow Ti^{2+} + 2e^{-}$ (2-15)

$2H_2O \rightarrow 2O^{-}{}_2 + 4H^{+}$ (2-16)

$Ti_2^{+} + 2O_2^{-} \rightarrow TiO_2 + 2e^{-}$ (2-17)

At Ti/Ti oxide interface:

$TiO_2 + 6HF \rightarrow TiF_6^{2-} + 2H_2O + 2H^{+}$ (2-18)

Meanwhile, the formation mechanism of the TiO_2 nanotubes at various stages is schematically illustrated by Figures 2.7(a)-(d). Initially, field-enhanced oxidation occurs at the Ti/Ti oxide interface by Eq. (2-15)-(2-17) when oxygen ions diffusion to the Ti layer as shown in Figs. 2.7(a). At the same time, competing field-enhanced oxide dissolution occurs at Ti/solution interface illustrated by Fig. 2.7(b). Specifically, fluoride-containing electrolyte reacts with TiO_2 to form TiF_6^{2-} as described by Eq. (2-18). Moreover, small pores are generated and spread uniformly over the surface of the film under an electric field. When the pore to pore distance achieves a suitable value at which the electric field of each pore would not affect each other, the distribution of electric-field strength would change.

As a consequence, under increased in local field strength at the bottom of the pore in conjunction with low dissolution rate at the sidewall, highly-order pore structures were formed as shown in Figure 2.7(c). Finally, in the growth stage, fully developed TiO_2 nanotube arrays are shown in Figure 2.7(d). Field- enhanced dissolution developed the depth of the pore to tube. Therefore, the steady-state nanotubes morphology was created.

2.3.3 Key parameters for controlling the growth of the nanotubes

Summarizing anodic oxidation technique, the key parameters to be considered when anodized TiO_2 nanotube and hybrid structures are the following:

Electrolyte

The electrolyte plays a crucial role in the growth of anodized TiO_2 nanotubes, as previously discussed. The main distinction is between aqueous and organic-based, where the water content is an important rule to limit dissolution of the oxide. Moreover, the pH of the solution is also important, considering the higher dissolution rate of the oxide in an acid environment. As shown schematically in Figure 2.8. While the pore bottom is at a low pH, the pore mouth (top of nanotubes) remains under a protective environment (higher pH) by using chemical buffer species [NH_4F/ $(NH_4)_2SO_4$]. The rapid rate of the TiO_2 dissolutions in the first generation of nanotube was reduced by replacing the HF acid [70] with less aggressive solutions containing fluoride salts, and raising the maximum thickness up to 2-3μm. [75] This is one of the reasons why dissolution was reduced of the TiO_2. If the anodic oxide is at its lowest when using fluoride salts (some of them have basic hydrolysis) instead of hydrofluoric acid.

Mechanical stirring system

The mechanical stirring was sometimes used to accelerate the reaction rate for nanotube growth. In addition, mechanical stirring also affect the inner tube morphology of TNAs. Figure 2.9 shows the schematic diagram of the formation of the tube spatial periodicity under different conditions: (a) without stirring; (b) at medium stirring rate; (c) at high stirring rate [82]. The smoothing effect of the tube inner surface and the acceleration of the growth are due to the redistribution of the F- anions in the nanotubes. Based on the experimental results, the mechanism has been discussed with the consideration of the local reactions and transport processes of the main reaction species.

Under this interpretation, the current oscillation and the morphology change in the pore are attributed to the redistribution of the ionic species by the fluctuation in the tube layer when there is no stirring. They can be significantly influenced by the convection above the tube layer and the slow transport process in the tubes with the existence of mechanical stirring.

Temperature

The temperature of the electrolyte affects the chemical dissolution and electrochemical dissolution and electrochemical etching rate in the growth of the nanotube arrays via anodic oxidation of titanium. For example, Grimes reported nanotube arrays were grown with a constant 10 V anode potential in an electrolyte of acetic acid plus 0.5 % HF mixed 1:7 ratio and kept at each of different electrolyte bath temperature: 5℃, 25℃, 35℃, and 50℃. Table 2.1 shows the variation in 10 V wall thickness and tube length as a function of anodizing temperature .Figure 2.10 shows the FE-SEM images of morphology of TiO_2 nanotubes fabricated by anodizing at 10 V at (a) 5℃ and (b) 50℃. The pore diameter is essential the same (22 nm) for the 10 V anodized TiO_2 nanotube arrays at these different temperatures.

Results show that with decreasing anodizing bath temperature the wall thickness increases from 9 nm at 50℃ to 34 nm at 5℃, confirming the trend of the increasing nanotube wall thickness with decreasing temperature.[83]

2.3.4 Application on DSSCs of TiO_2 nanotubes arrays

Recently, research has been directed toward synthesizing structures with a high degree of order than the random assembly of nanoparticles. A desirable morphology of the films would have the mesoporous channels or nanorods aligned parallel to each other and vertically with respect to the glass substrate. This would facilitate charge diffusion in the pores and the mesoporous films, giving easier access to the film surface, avoiding grain boundaries and allowing the junction to be formed under better control.

One approach to fabricate such oxide structures is based on anodized TiO_2 nanotubes by Frank and co-workers [84]. They reported that the nanotubes and the nanoparticles in conventional DSSCs have similar transport properties (the electron has to diffuse though the oxide and reach the electrode to feed the circuit), however lower recombination occurs in the nanotubes because of a higher charge collection efficiency. In addition, the nanotubes harvest the light more efficiently than conventional DSSCs, because of stronger light scattering effecting. However, their use in DSSCs still far from optimized.

2.3.5 Challenge of TiO_2 nanotubes arrays on DSSCs

From the literature, it has known crystalline nanotube or nanowire based on TiO_2, in contrast with the random transport path in nanoparticle, have been investigated to improve electron collection. Then, there are challenges existing and need to overcome. One of challenges is that 1-D nanostructures have a lower internal surface area than mesoporous films. In DSSC application, the reported efficiency of TiO_2 nanotube based DSSC is generally much lower than DSSCs based on nanoparticles and amounted to 0.61%-2.9% [85,86,73,87]. The possible reason is that the internal surface area of nanotube based photoanode is much smaller than that of nanoparticles due to a lower dye loading and sunlight adsorption.

2.3.6 TiO_2 hybrid structure (TNWs/TNAs)

There are various methods fabricating TiO_2 which can be organized according the templates used during the experiment. Sol-gel processing which transcription used organo-gelators as templates [88,89], seed growth [90], deposition into a nanoporous alumina templates, and hydrothermal processes [91].

Among them, anodizing oxidation method is better due to the highly order arrays. Anodizing oxidation carries on producing a long TiO_2 nanotube arrays in viscous electrolyte, and the TiO_2 nanowires are found [92]. In 2012, Haijun and the coworkers [93] found the TiO_2 nanobelts exist between TiO_2 nanowires as shown in Figure 2.11

2.3.7 Anneal treatment for TiO_2 material

Titanium dioxide ($TiO_{2)}$ can exist in three distinct crystalline polymorphs: anatase, rutile, or brookite crystalline phase, respectively shown in Figure 2.12 [94]. From Figure 2.12, all three crystal structures are made up of distorted octahedra, each one representing a TiO_6 unit, where each Ti^{4+} is at the center of the unit and coordinates six O2- ions. The manner in which the octahedra assemble to form a TiO_6 based chain is different and characteristic of each polymorph. In these three phases, rutile and anatase are the most commonly synthesized phase. Anatase and brookite are metastable phases and convert into rutile at high temperature, usually above 600 ℃ [95]. Table2.2 lists some of the key properties [90,96] of the three TiO_2 polymorphs. Both rutile and anatase have a tetragonal crystal structure, where brookite has an orthorhombic symmetry. Rutile is the densest phase and has the highest refractive index, while anatase is characterized by the widest band-gap (~3.2 eV) [92]. The properties (density, band-gap, and refractive index) of brookite fall between those of rutile and anatase.

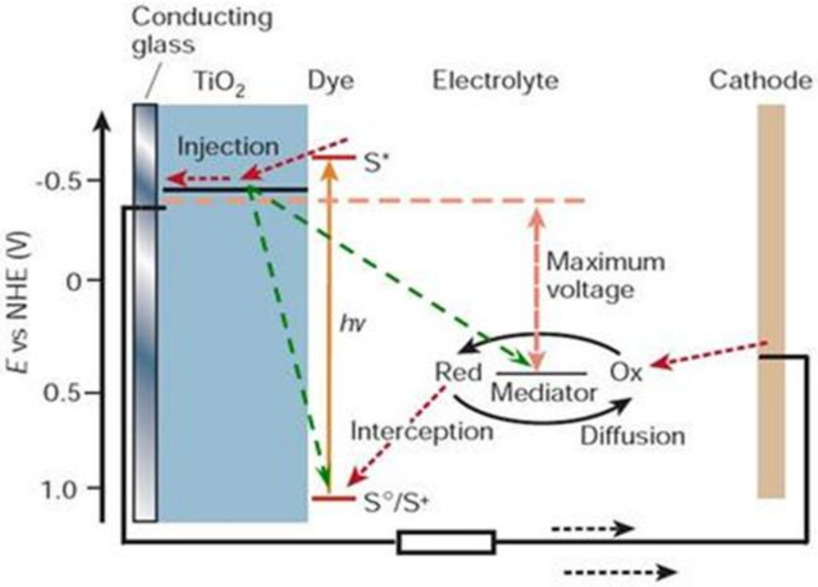

Figure 2.1 Schematic of DSSC operation [1]

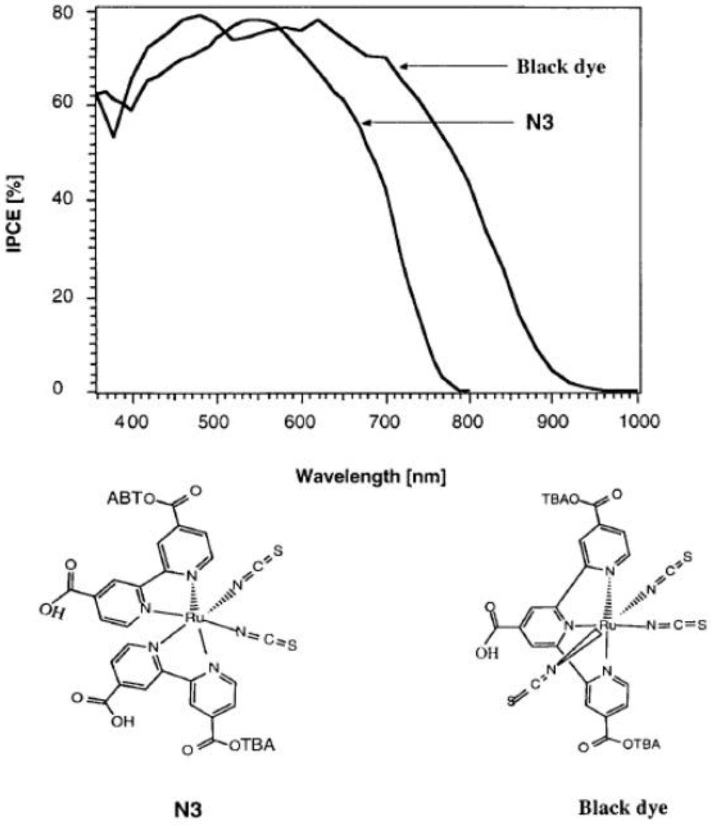

Figure 2.2 (a) Spectral response curves of the photocurrent for the DSSC sensitized by N3 and the black dye. (b) The chemical structures of N3 dye and black dye. [97]

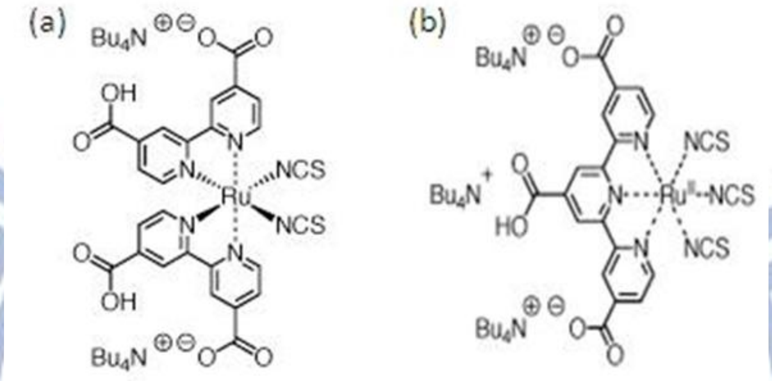

Figure 2.3 Chemical structures of N719 dye and N749 (black dye) [39]

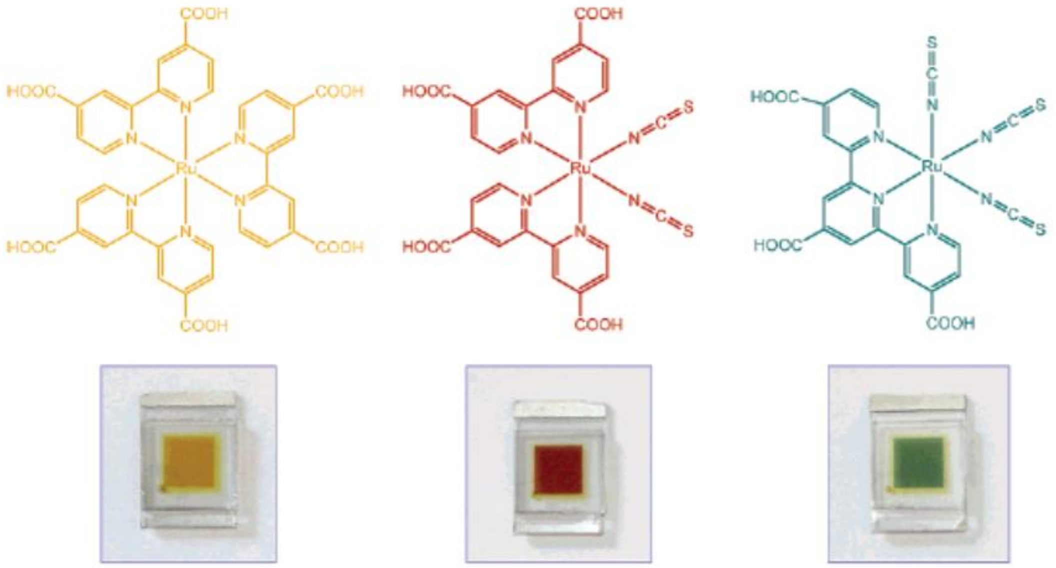

Figure 2.4 Structures of the ruthenium sensitizers RuL$_3$ (yellow) *cis*-RuL$_2$(NCS)$_2$ (red) and RuL’ (NCS)$_3$ (green), where L=2,2’-bipyridyl-4,4’-dicarboxylic acid and L’=) 2,2’,2”-terpyridyl -4,4’,4”-tricarboxylic acid. The lower part of the picture shows nanocrystalline TiO$_2$ films loaded with a monolayer of the respective sensitizer.[98]

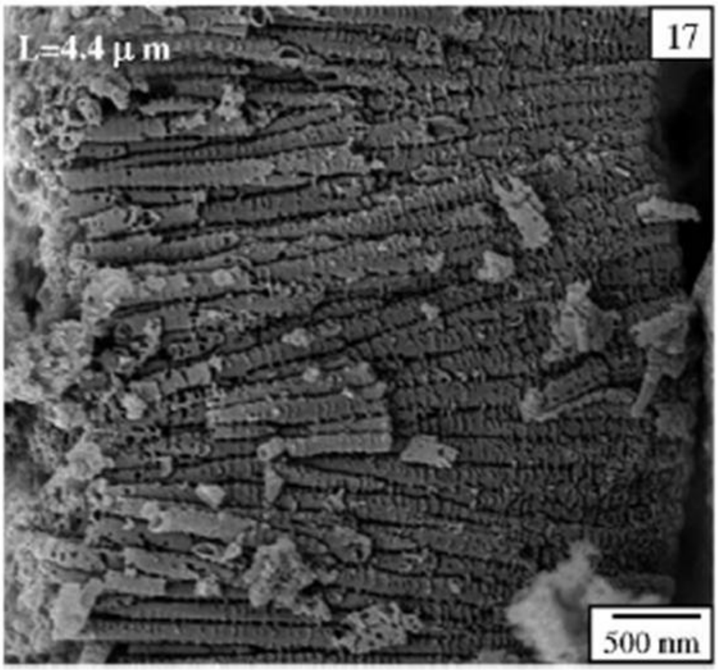

Figure 2.5 Lateral view of the nanotubes formed in 0.1 M KF, and 1 M H_2SO_4, and 0.2 M citric acid solution (25 V, 20 h)[72]

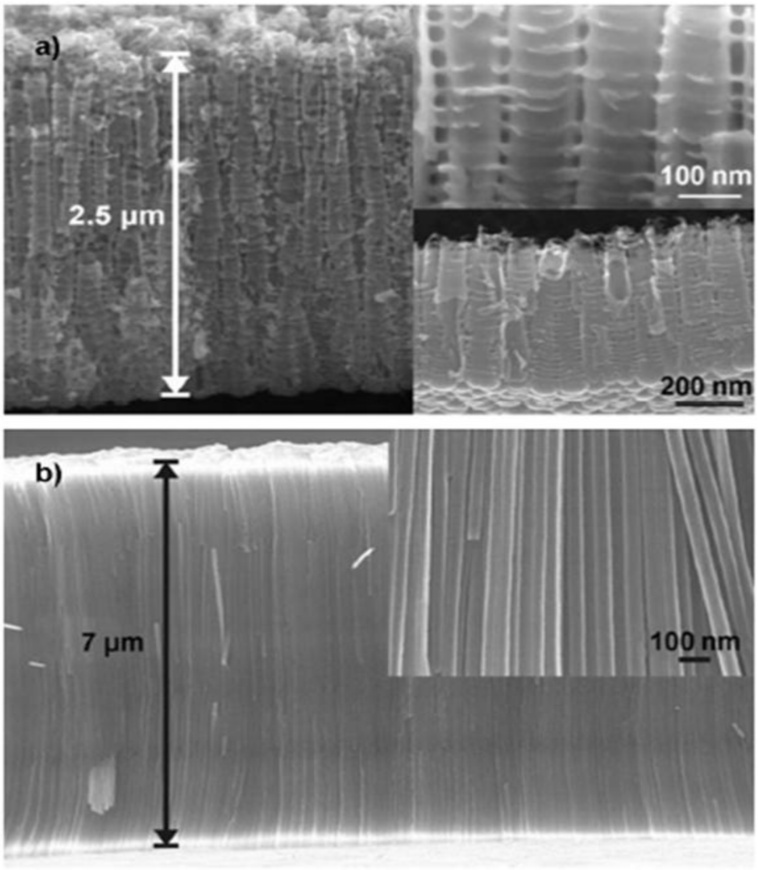

Figure 2.6 A comparison between SEM cross-sectional images of nanotubes in (a) an aqueous based and (b) organic electrolyte [74]

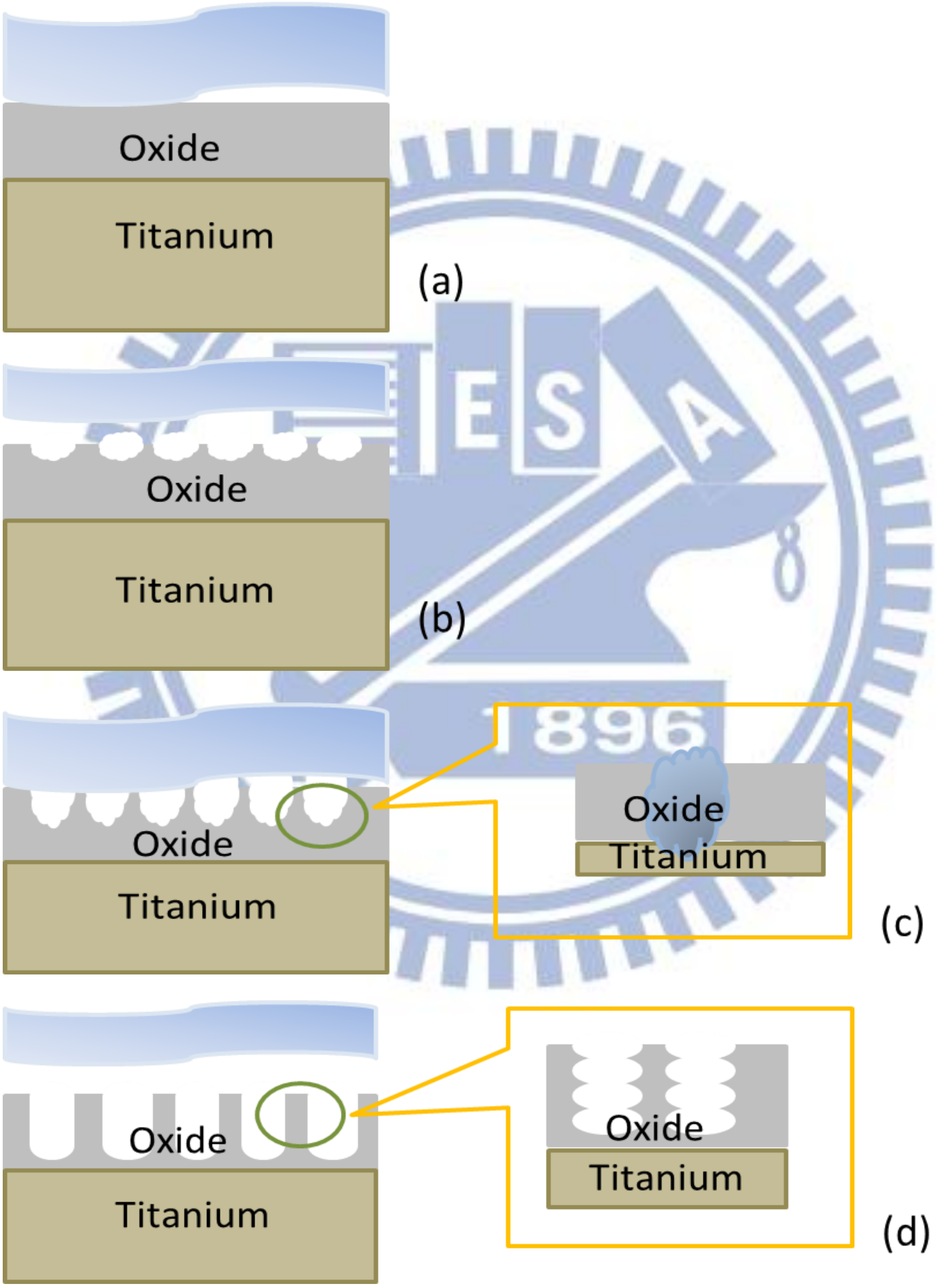

Figure 2.7 Schematic diagrams illustrating the formation mechanism of TiO_2 nanotubes

structures (a) oxide layer formation, (b) semicircle pores formation on the oxide film, (c) growth of the semicircle pores into scallop shaped pores, and (d) fully developed nanotube arrays.

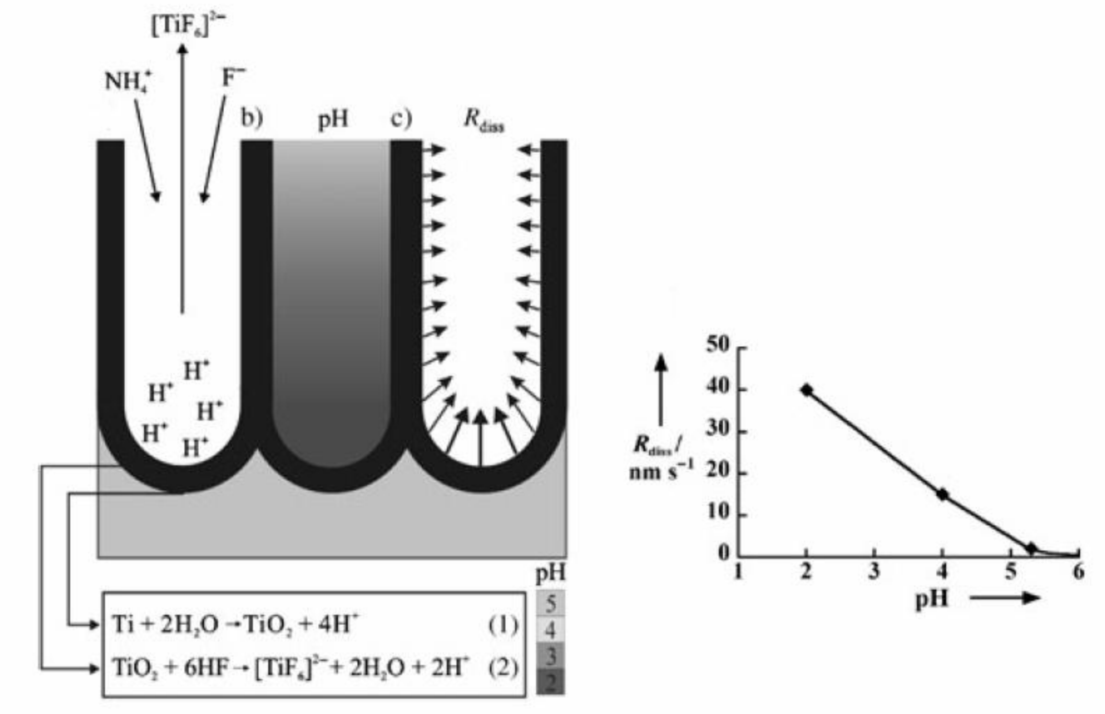

Figure 2.8 Schematics of the pH profile developing within the tubes during the anodization process according to Macak et al. [70]

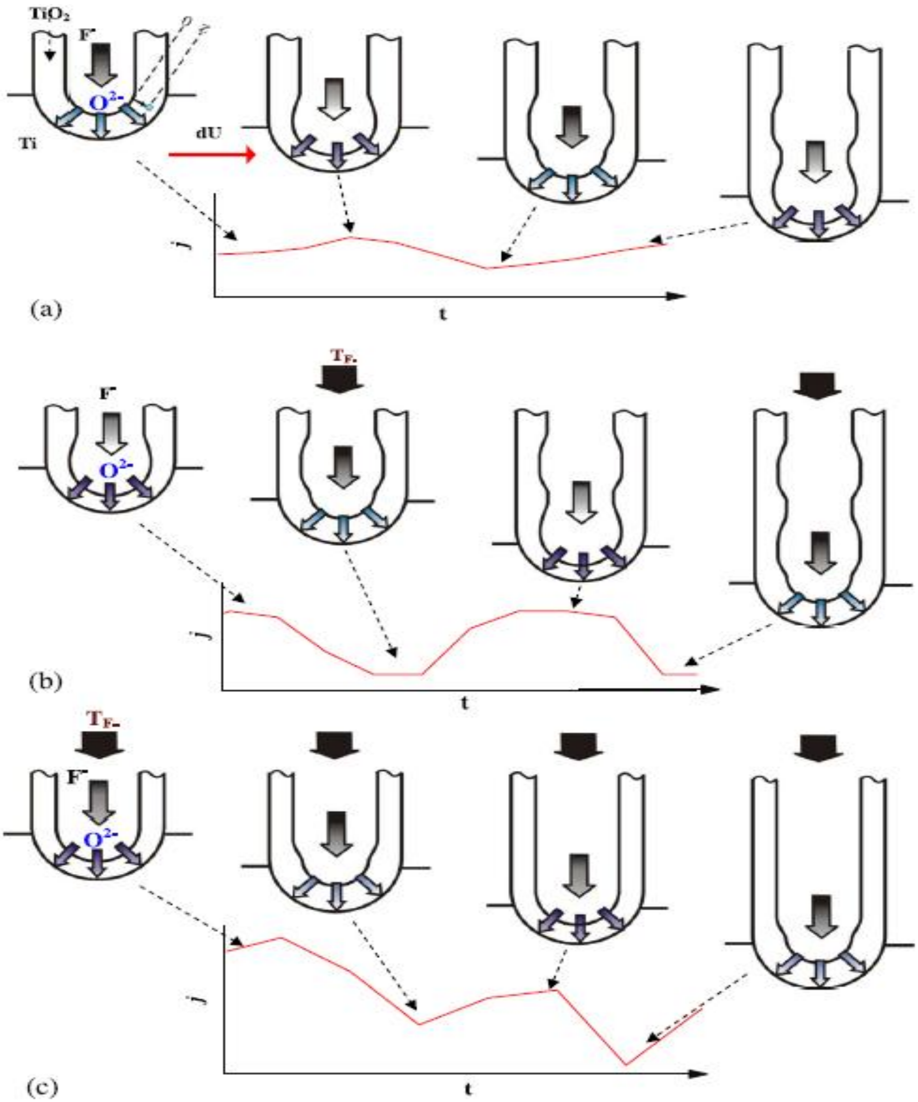

Figure 2.9 Schematic diagrams of the oscillation mechanism: formation of tube spatial periodicity and corresponding current behavior under different conditions: (a) without stirring; (b) at medium stirring rate; (c) at high stirring rate or with periodic modulated voltage. [80]

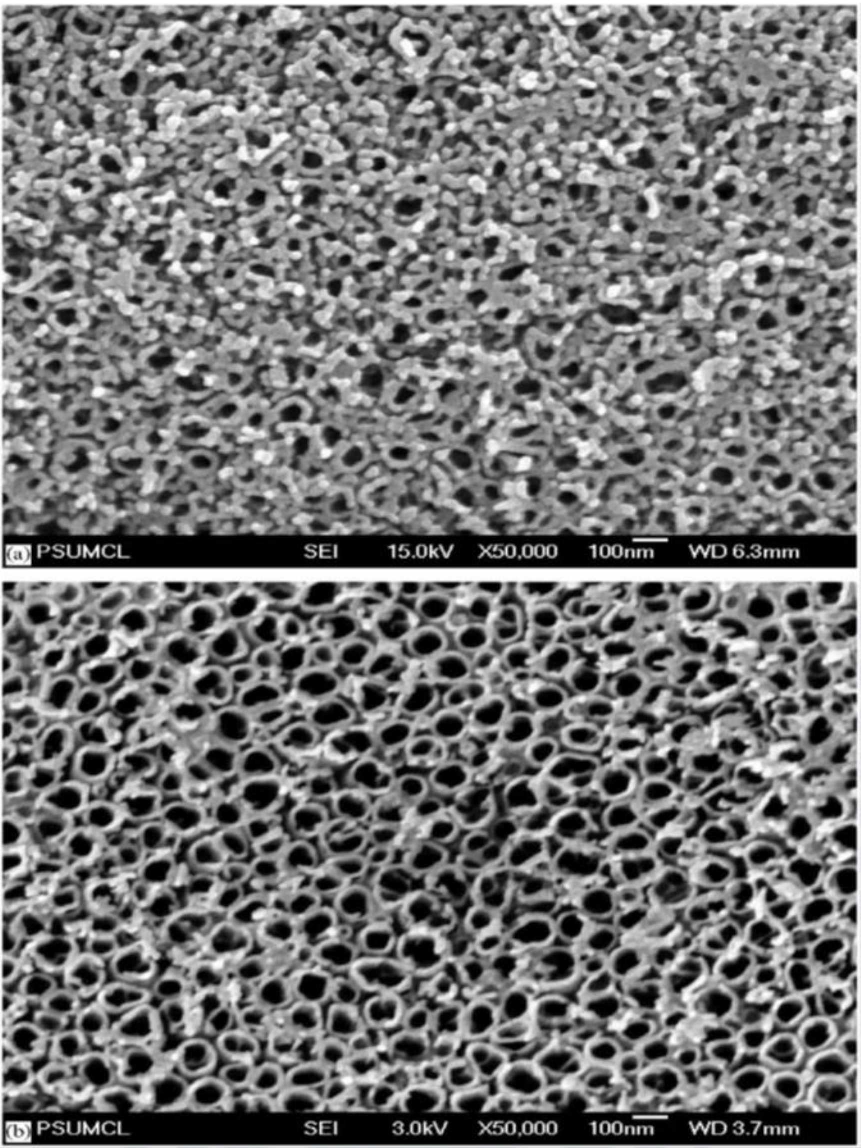

Figure 2.10 FE-SEM images of nanotube arrays anodized under 10V at: (a) 5℃ with an average wall thickness of 34 nm, and (b) 50℃ with an average wall thickness of 9 nm. The pore size is 22 nm for all samples. [81]

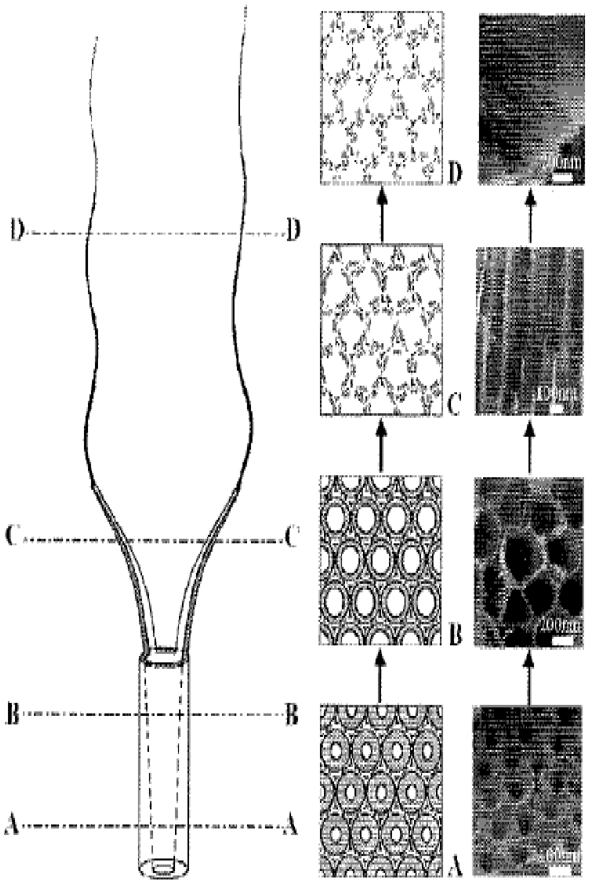

Figure 2.11 Schematic illustration of TiO$_2$ nanowires/ nanobelts standing on TiO$_2$ (Right), nanotube arrays section drawing of given regions (Middle), and FE-SEM images corresponding to section drawings (Right) [92]

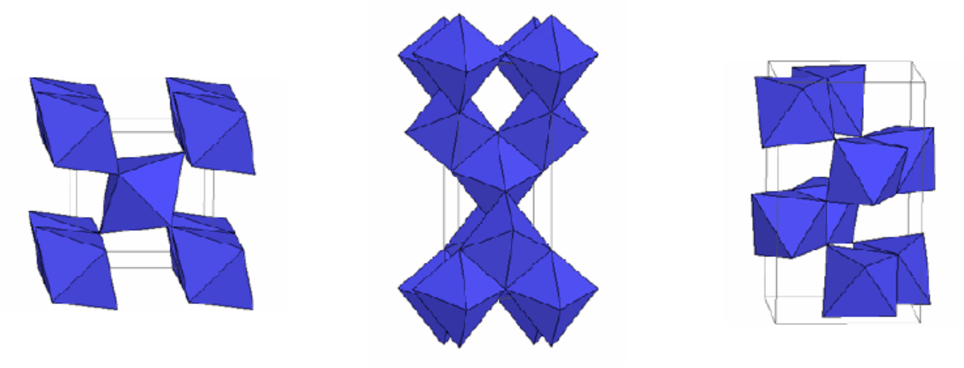

a) rutile b) anatase c) brookite

Figure 2.12 Different TiO_2 crystal structures: **(a)**rutile, **(b)**anatase, and **(c)** brookite. Images courtesy of Joseph R. Smith, University of Colorado [90,92]

Table 2.1 Average wall-thickness and tube-length of 10V titanium nanotube arrays anodized at different bath temperatures [81].

Anodization temperature(℃)	Wall thickness (nm)	Tube length (nm)
5℃	34	224
25℃	24	176
35℃	13.5	156
50℃	9	120

Table 2.2 Different TiO_2 polymorphs and some of their physical properties[90,92]

	Rutile	Anatase	Brookite
Crystal System	tetragonal	tetragonal	Orthorhombic
Density (g/cm3)[90,92]	4.13-4.26	3.79-3.84	3.99-4.11
Band-Gap (eV)[92]	3.0	3.2	3.11
Refractive Index[92]	2.72	2.52	2.63
Melting Point(°C)	1855	Converts to rutile	

Chapter 3 Experimental Section

3.1 Materials

Materials for fabricating TiO_2 nanotube arrays structure (TNAs) and hybrid structure (TNWs/TNAs)

1. Titanium foils 99.9 % purity, 0.5mm thickness and 0.127μm thickness. Sample size 0.28 cm^2
2. NH_4F from SHOWA for contributing F^-.
3. Ethylene glycol (EG) from SHOWA for a high viscosity electrolyte. The structure is :

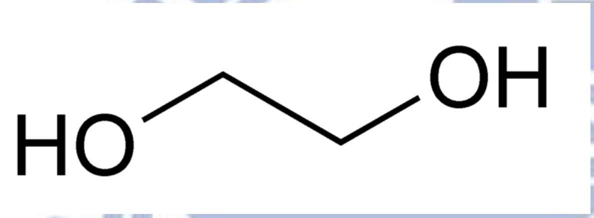

Materials for DSSCs

1. Titanium tetrachloride ($TiCl_4$) (from SHOWA) is for post-treatment of TiO_2 film
2. Titanium foil 99.9 % purity, 0.5mm thickness and 0.127μm thickness.
3. Ethanol (C_2H_5OH) (from ECHO) is used as a solvent for dye solution and the chemical structure is:

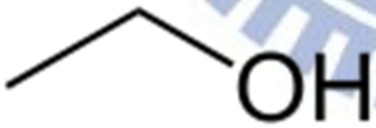

4. Surlyn® (SX1170-60) (from SOLARONIX) is used as the spacer and sealing material
5. N719 dye from UniRegion Bio-Tech and the chemical structure is:

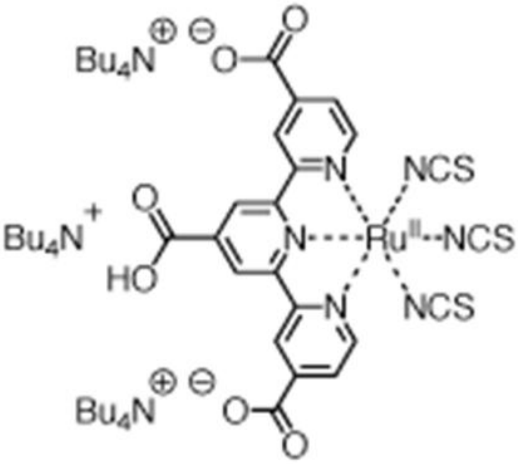

Materials for electrolyte

1. Lithium iodide (LiI) from MERCK

2. Iodine (I_2) from SHOWA

3. 1-methylbenzimidazole from Alfa Aesar and the chemical structure is:

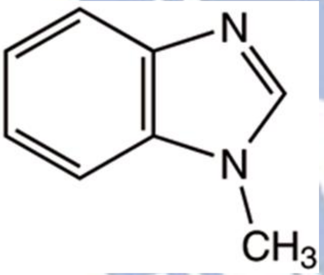

4. Guanidine thiocyanate from Alfa Aesar and the chemical structure is:

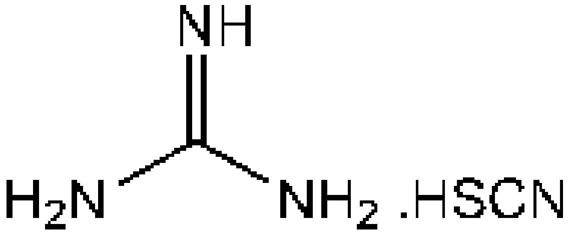

5. 1-Methoxypropionitrile (from Alfa Aesar) is a solvent for the liquid electrolyte and the chemical structure is:

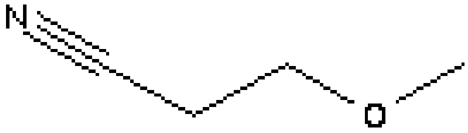

3.2 TiO_2 films Preparation

3.2.1 TiO_2 nanotube arrays film (TNAs)

Titanium foils (99.9% purity) of 0.5 mm or 0.127 mm thickness with a sample size of 0.28cm^2, were used as the substrate for forming TiO_2 layer by anodic oxidation. Prior to anodization, Ti foil was ultrasonically cleaned by distill water, rinsed by acetone, and then dried by a purging N_2 gas. The schematic diagram of anodizing reaction system is illustrated in Figure 3.1.

All anodizing experiments were carried out at room temperature using a two-electrode electrochemical cell consisting of a stainless steel foil (SS304) as the cathode and a Ti foil as the anode, at a constant DC potential. The electrolyte: 0.5 wt% NH_4F dissolved in the ethylene glycol (EG) solution with 1 wt.% H_2O. Anodizing conditions are (1) 40 V for 30-40 min and (2) 30 V for 4h under stirring at 300rpm. The working layer of DSSCs in the study was fixed at 12µm, unless stated otherwise.

3.2.2 TiO_2 hybrid film (TNWs/TNAs)

A hybrid structure composite of TiO_2 nanotube and nanowire were fabricated by using electrolyte consisting of EG and water (99:1 in wt.%) with 0.5 wt.% NH_4F. The conditions of anodizing voltage and processing time were designed to elucidate the formation mechanism of TNWs/TNAs and also fixed in the same thickness to compare the efficiency performance. The electrolyte: 0.5 wt % NH_4F dissolved in the ethylene glycol (EG) solution with 1 wt.% H_2O. Anodizing conditions are (1) 40 V for 2h and (2) 30 V for 8h. The working layer of DSSC was fixed at 12µm. Otherwise, we increase the processing time at anodizing voltage of 40 V from 2 h to 5 h in order to examine the transition from nanobelts to nanowires and thickness reaches 15 µm.

3.2.3 Post-treatment for TiO_2 films

$TiCl_4$ treatment

The post-treatment was done by immersing the TiO_2 anode into the 0.1 M $TiCl_4$ water solution for 30 min in ice bath to form small TiO_2 particles on the wall of TNAs and TNWs/TNAs for increasing the surface area. This can improve the charge transfer between TiO_2 films and dye adsorption.

Annealing for TiO_2 films

After $TiCl_4$ treatment, TiO_2 anode was sintered at 400℃ for one hour to transform the TiO_2 film into anatase phase. For TNAs and hybrid structures, the thermal annealing was performed in O_2 ambient at 400°C for 1 hour under a heating rate of 2°C/min. A tungsten wire heater was rolled around the quartz tube to create a homogeneous temperature in the furnace.

3.3 DSSC fabrication

The TiO_2 photoanode was immersed in a 3×10^{-4}M N719 dye ethanol solution at room temperature for 24 hours for dye adsorption. After sensitized, the TiO_2 photoanode was dipped into ethanol to remove extra dye which did not adsorb on the TiO_2 surface. DSSC was fabricated by sealing the dye-sensitized TiO_2 photoanode and Pt-sputtered counter electrode around 100℃ with a hot-melt sealing foil. The hot-melt sealing foil was also served as a 60 μm spacer. There are two tiny holes on the Pt-sputtered counter electrode for injection of electrolyte.

The electrolyte composition was 0.5M LiI, 0.05M I_2, 0.2M 1-methylbenzlmidazole, and 0.5M guanidine thiocyanate in 1-methoxypropionitrile solvent. The electrolyte was injected into the cell through two tiny holes on the counter electrode. After the extra electrolyte was removed, the two tiny holes were also sealed by the hot melt sealing foil with a normal glass. Figure 3.2 illustrates the schematic diagram of DSSC fabrication process.

3.4 Characterization techniques

3.4.1 Morphology and microstructure characterization of TiO_2 nanostructure

The surface and cross-section morphology of TNAs, TNWs, and TNP were observed by a field emission scanning electron microscope (FESEM) (HITACHI-S2500 JSM-6500F). FESEM is a powerful analytic tool for characterizing the microstructure down to several ten nanometers. The detector gathers secondary electrons signal, and transfers into a SEM photo through an amplifier. In practice, a metal layer (ex. Au, Pt) is coated on the samples to alleviate charging effect. FESEM was operated at an accelerating voltage at 15.0 KV. The thickness of TiO_2 films were examined by focus ion beam microscope (FIBSEM), which was carried out at an accelerating voltage at 5.0 KV.

An X-ray diffractometer (XRD) (Siemens Diffractometer, D5000) with Cu Kα (λ=1.5405Å) radiation was employed to analyze the crystal structures of TNAs and TNWs/TNAs.

3.4.2 Dye adsorption measurement

The surface areas of the TiO_2 film were measured by dye (N719, dye, Solaronix) adsorption, which is a commonly used method in DSSC applications [99]. Specifically, the amount of dye adsorption was determined by desorbing the dye from the TiO_2 films into 5mM NaOH aqueous solution. The quantification was based on the dye’s maximum absorption values at 505 nm in the dye-desorbed NaOH solutions as measured by an UV-visible light spectrometer (Evolution300), using a dye solution of concentration 5×10^{-3} mM as a reference.

3.4.3 Conversion Efficiency

The AM1.5 solar simulator (Newport 3A) was used as the light source, and the incident light spectrum was AM1.5, 1 sun (100mW/cm^2) calibrated with standard Si solar cell (ORIEL). I-V curve was recorded with Keithley by scanning DSSC from -0.05V to 0.85V, and the photoelectrochemical characterizations of DSSCs were carried out by computer calculation with the active area 0.28cm^2.

3.5 Experimental flow

The experiment design and flow chart are schematically illustrated in Figure 3.3. The working layer of TiO_2 films were fabricated by anodic oxidation technique described in Section 3.2. Subsequently, TiO_2 films were treated with $TiCl_4$, followed by annealing, then immersing into a N719 dye solution. Finally, the DSSCs were assembled and packaged as described in Figure 3.2. The DSSC performance such as I-V curve was characterized.

For the film properties such as surface area and morphology, TiO_2 films were immersed into the dye solution for dye adsorption. The dye was then desorbed into NaOH water solution for the dye adsorption measurement using an UV-visible spectrometer. The morphology of TiO_2 films under various voltages and processing time was observed by SEM.

By UV-visible spectrum, the dye adsorption amount could be quantified. The TiO_2 electrodes with light-scattering layer after $TiCl_4$ post-treatment were dye-sensitized and fabricated into DSSCs for efficiency measurement. The relationship between morphology and DSSC performance will be examined and discussed.

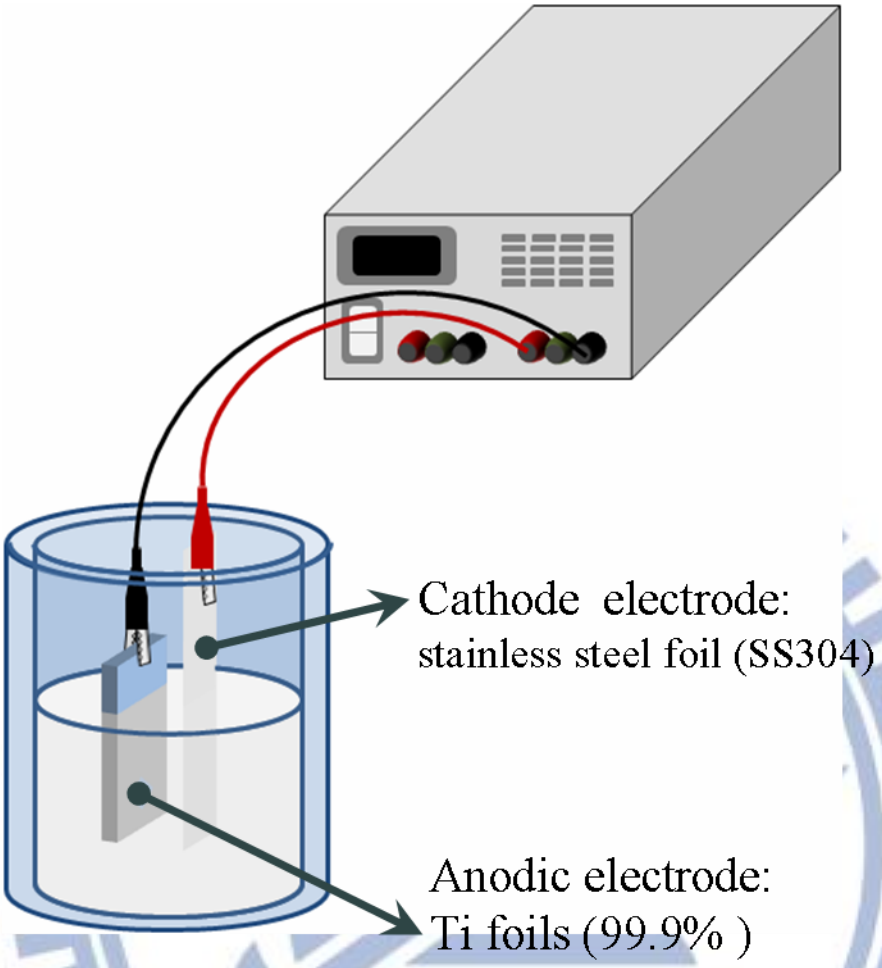

Figure 3.1 Schematic diagram of anodization reaction system.

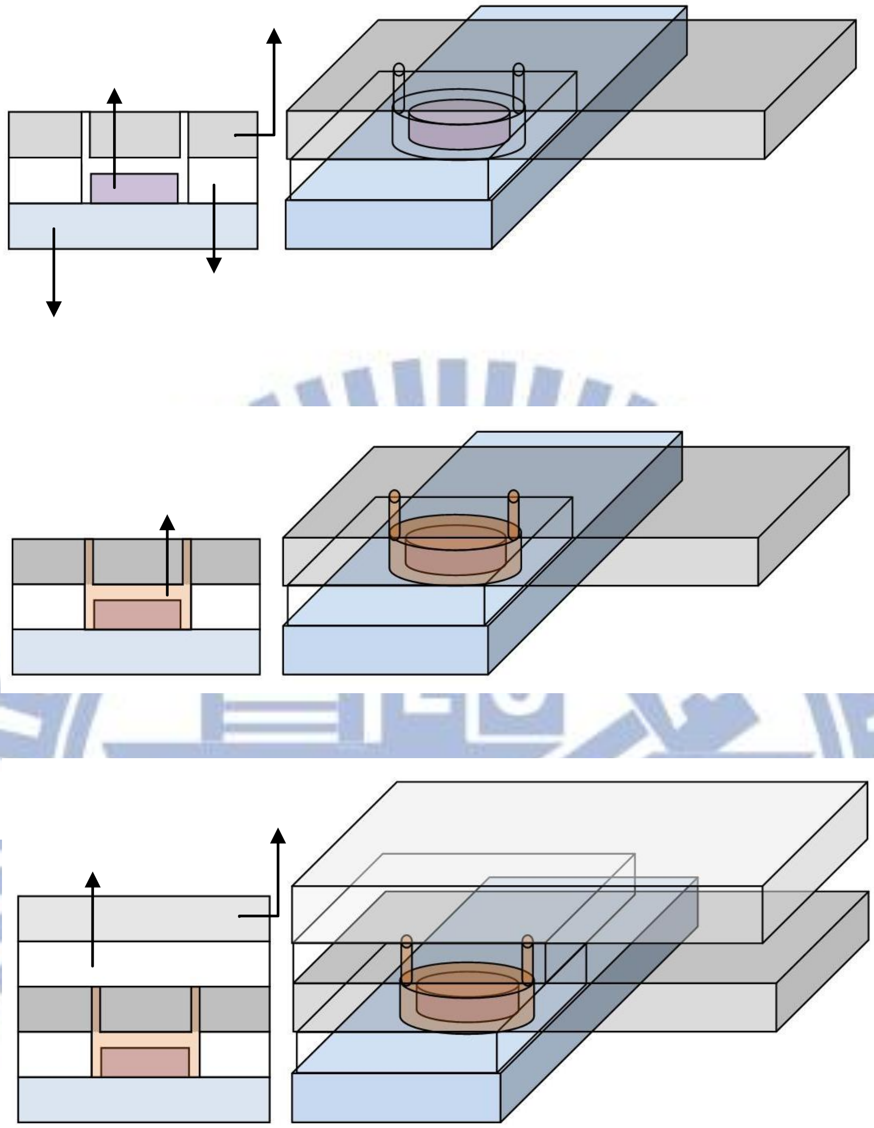

Figure 3.2 The DSSC fabrication process.

(a) Sealing the dye-sensitized photoanode and Pt-coated counter electrode.

(b) Injecting electrolyte injection through the injection holes,

(c) Sealing the injection holes on the counter electrode.

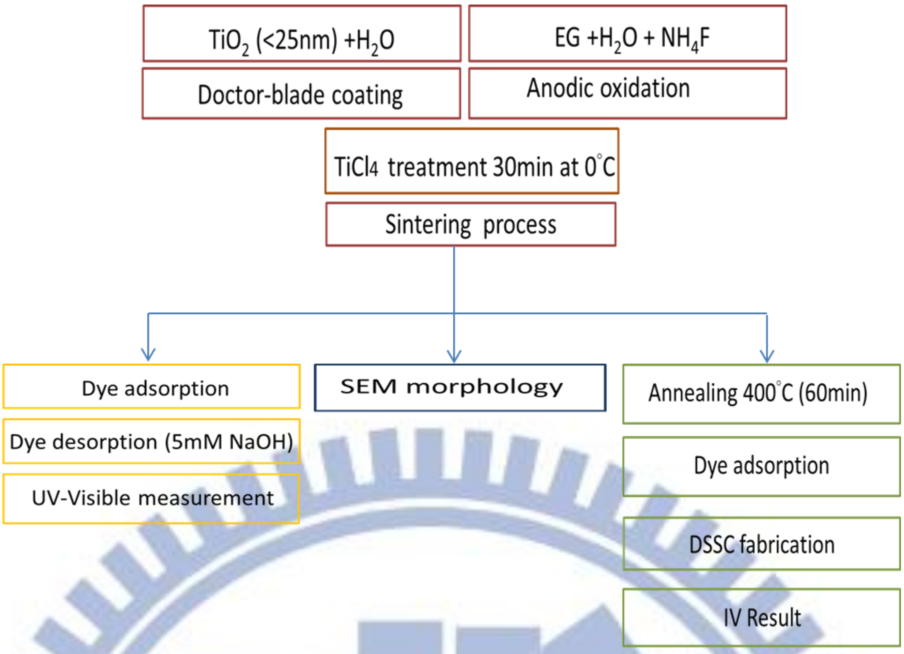

Figure 3.3 Diagram of Experimental Design and Flow: sample preparation and characterization

Chapter 4 Results and Discussion

Two types of TiO_2 nanostructure, *i.e.* TiO_2 nanotubes (TNAs) and TiO_2 nanowires on TiO_2 nanotubes (TNAs) (TNWs/TNAs hybrid structure) will be fabricated by anodizing titanium metal foil in this study. The parameters of anodization include anodic voltage, processing time, and mechanical stirring, which affect the diffusion of ionic species and electric field, leading to different morphologies. The DSSC performance of TNWs/TNAs hybrid structure will be measured and compared with TNAs and conventional TiO_2 nanoparticle film.

4.1 Influence of anodization parameters

4.1.1 Influence of anodizing voltage and processing time without mechanical stirring

Figures 4.1(a) to (c) illustrate the SEM images of TiO_2 films prepared by various anodizing voltages from 30 V to 50 V without stirring, in a 0.5 wt.% NH_4F solution under a constant anodizing time of 0.5 h. For the case of 30 V as shown in Figure 4.1(a), the surface morphology shows the highly ordered TiO_2 nanotube arrays with a wall thickness of 56 nm. When the anodizing voltage was increased to 40 V, the wall thickness was reduced to 32 nm. For applying voltage of 50 V, the wall thickness was 26 nm as illustrated in Figure 4.1(c).

In the parallel electrode, the increases voltage induces a stronger electron field. The ions would gather due to the electron field. It can be related to the capacitor, the $C=q/V= \varepsilon*A/d$, the ions concentrations is the same as the charge number; the capacitor value is the same. Thus, the charge will increase with the applied voltage. Moreover, fluorine concentration originated from NH_4F induces the electrochemical etching. The increased voltage influences the concentration F^- ions on electrode surface. Therefore, the higher anodizing voltage, the thinner wall thickness of the nanotube become due to a higher etching rate in the top section. [79]

Recently, Hsu *et al.* [100] fabricated TNWs/TNAs hybrid structures by using a one-step anodization method without mechanical stirring. At an anodizing time of 30 min without stirring, it can be observed the pure TiO_2 nanotube arrays (TNAs) and the steady-state growth of TNAs length is approximately ~0.4 μm/min at 40 V before the emergence of nanowires. This suggests that the H^+ concentration is maintained at the bottom during the chemical drilling [75] because the high-viscosity EG electrolyte limits the ionic diffusion of the electrolyte with a protective environment maintained the pore walls and at the pore mouth during the chemical drilling. With the processing time increased, the mouth of nanotube became fragile. Finally, the wall thickness was too thin to hold and collapse on the tube mouth as illustrate in Figure 4.2.

In this study, we further examine how the tube is changed to nanobelts, then nanowires under the anodizing processing conditions. Figure 4.3 illustrated the condition of required anodizing voltage and processing time (shaded zone) for forming forming TNWs/TNAs (white zone) and the excluded shaded zone for forming TNAs only.

In order to observe the evolution of TiO_2 film, we fixed the experiment at a constant anodizing voltage of 40 V and enlarged the processing time. Figure 4.4(a)-(c) show the SEM images for surface morphology of TiO_2 films prepared under 40 V using an anodizing time of 0.5h, 2h, and 4h respectively. The length of TNWs/TNAs reach in 10-11μm when anodizing time is 0.5h. Further, it reaches 12μm at 2 h, 15 μm for 4 h and 16μm for 5 h.

The nanowire still etched under the anodizing, the width of nanowire was changed in a period. The width of nanowire is ~70 nm at the voltage 40 V for 2h. As the treatment time was further increased 3 h, 4 h, and further increased to 5 h, the width of nanowire became ~45 nm, 70nm, and ~45 nm as show in Figure 4.5. The evolution shows the nanowire would be etched until vanish. Meanwhile the tube wall collapsed and inner diameter increased from ~80nm to ~100nm. The Figures 4.6(a)-(b) illustrate how the nanobelt divide into nanowire, and the growth and decline affect the growth rate of TNWs/TNAs under 40 V.

Both the applied electric field and processing time play important roles in the formation of TNWs/TNAs. The emergence of nanowire was controlled by processing time and voltage. The flux of ions in the presence of electric field can be expressed as:

$$J_i = -D_i \frac{\delta c_i}{\delta x} - u_i c_i E \qquad (4.1)$$

Where J_i is the flux of species i of concentration c_i in direction x, $\frac{\delta c_i}{\delta x}$ is the concentration gradient, D_i is the diffusion coefficient, u_i is the mobility of species i, and E is the electric field strength. According to the formula, we can understand the ion transport in the electrolyte is significantly influenced by electric field. The ion migration is contributed by the applied electric field and the process of ion diffusion under a concentration gradient.

As a result, the TNWs/TNAs hybrid structure was formed only under anodizing voltage of < 60 V as shown in Figure 4.2, with longer treatment time for lower voltages. At voltages higher than 60V, no formation of nanowires was observed. In this study, we further identify the required processing time for applied voltage down to 25V.

The formation mechanism of TNWs/TNAs without mechanical stirring has been proposed by Hsu et al. [100]. TiO_2 nanowires are found to evolve and form on the top of the TNAs through several stages. Figure 4.2 (a) to (d) [100] show the schematic diagrams along with their corresponding surface morphology images for four key stages in the TNWs/TNAs formation mechanism. First, as the anodic titanium oxide reaction began, the order TNAs was formed, resulting from the field-enhanced chemical drilling by high H^+ concentration at the pore bottom of the tubes, in conjunction with a protective environment maintained along the pore walls by the highly viscous EG solution.

As the anodic oxidation reaction proceeded, field-enhanced dissolution in the tube bottom still prevailed to further increase the aspect ratio (highest/diameter) of the TNA at this stage, as Figure 4.2 (a). However, the wall thickness near the tube mouth shown in Figure 4.2 (a) became smaller due to enhanced dissolution of TiO_2.

In the electrolyte, the migration of F^- toward the electric field of the bottom electrode is inhibited by highly viscous solution. This results in F^- concentration much higher at the tube bottom [101].With the presence of water in our case, the hydrogen ions further boot the chemical dissolution reaction of forming TiO_2 nanotube [102]:

$$TiO_2+6F^-+4H+\rightarrow TiF_6^{2-}+2H_2O \tag{4.2}$$

The distribution of the hydrogen ions also result in the wall thickness near the tube mouth was thinner than the foundation as illustrated in Figure 4.2(b)

Meanwhile, the inner surface of the tubes was rough without mechanical stirring in the electrolyte bath as reported by Liu, Shen, and Tao.[103] Thus, the inner tube diameter of the TNAs was not uniform, as schematically illustrated in the inset 1 of Figure 4.2(b) and marked by arrows.

Under an anodizing condition including the specific voltage and processing time, in which the wall thickness at the tube mouth is < 10nm, the area of the inner wall thickness near the top of the TNAs would be etched through by the increased TiO_2 dissolution reaction as illustrated in inset 2. As the processing goes by, the strings of through holes on the tubes in the top TNAs, were formed from top to bottom, along the F^- ions migration direction under electric field, as shown in Figure 4.2(b)

After the strings of through holes on the tube form, the tube wall would initial and propagate downward. As illustrated in Figure 4.2(c), the holes near the top expand and became connected to split into nanowire. With the nanowire further electrochemically etched, resulting in the smooth wire edge and nanowire wire width of nanowire as illustrated in Figure 4.2(d). In addition, the collapsed nanowire on the TNAs, its length is ~5-10 μm.

In short a strings-of-through-holes model [100] is based on the enhanced TiO_2 dissolution reaction near the top section in conjunction with a threshold wall thickness of ~10 nm for forming nanowire and high thickness non-uniformity without a mechanical stirring. Four key stages in the TNWs/TNAs formation mechanism are: (a) thinning of the tube wall thickness with high roughness near TNAs mouths, (b) forming strings of through holes in the top section of TNAs, (c) splitting into nanowires, and (d) collapsing and further thinning of nanowire.

4.1.2 Influence of anodizing voltage and processing time under mechanical stirring

Figure 4.7 shows the inner diameter and wall thickness of TNAs near the top section prior to the emergence of nanowires, as a function of voltage and mechanical stirring. In these cases, a processing time of 0.5 h was used to ensure no formation of TNWs. Regardless the stirring, the wall thickness decreases from 20 nm to 8 nm with increasing voltage, while the tube diameter increases from 15-30 nm to 80-100 nm with increasing voltage. In specific, the wall thickness of nanotube top section without mechanical stirring is larger than that with mechanical stirring. Conversely, the tube inner diameter is larger in the cases with mechanical stirring as compared to those without mechanical stirring.

The stirring was driven by a stirring bar, which rotated the electrolyte between the electrodes, with a constant rate by controller. This resulted in uniform tube diameter and wall thickness. In contrast, thinner wall thickness near the top section was expected due to high F^- concentration when no mechanical stirring was used. Based on this study and previous work in this research group [100], the criteria of wall thickness for forming TNWs/TNAs structure is ~9-10 nm. This implies that the required time for forming TNWs/TNAs structure will be extended if mechanical stirring is used.

Figures 4.8 (a)-(d) illustrate the SEM images of the TiO_2 films prepared at 30 V in a 0.5wt% NH_4F solution for 4 h and 6h with mechanical stirring [(a) and (b)] and without stirring [(c) and (d)], respectively. The surface morphology in Figure 4.8 (a) shows highly ordered TiO_2 nanotube array at a processing time of 4 h with a tube diameter of ~50 nm and wall thickness of ~12 nm. However, TNWs/TNAs structure appeared when the processing time was increased to 6h, as illustrated in Figure 4.8(b), at which the wall thickness was ~9 nm presumably due to additional etching with time. In contrast, nanowires were observed at 4h without mechanical stirring as shown in Figure 4.8(c) due to its thinner wall thickness with a rough terrain at the same processing time. In addition, the edge of nanowires by anodizing with stirring seems to be smoother than those without stirring as shown in Figure 4.8 (d).

The anodizing under mechanical stirring takes consideration of the transport processes of ionic species (F^-, O^{2+}, and H^+), the stirring can induce the redistribution of anions in the convection layer as illustrated in Figure 4.9 [105].

When stirring is applied, F^- ions will move to the bottom of the tubes due to the diffusion and electric field Figure 4.10. [104] With the mechanical stirring, ions transportation can be significantly influenced by the convection layer near the top section of nanotubes as shown in Figure 4.10 [103] and the slow transport process (diffusion and field-aided transport) in the tubes. The convection above the tube provides the F^- ions to eliminate the TNWs on the top of nanotube and result in the delaying the emergence of the TNWs/TNAs. During this processing time, the length is enhanced with pure TNAs.

4.2 TiO_2 Morphologies on DSSCs

4.2.1 Morphology and thickness of TiO_2 films

In this study, the thickness of three different TiO_2 morphologies, namely TNWs/TNAs, TNA, and TiO_2 nanoparticle films were kept the same at 12 μm, while the inner diameter size and tube thickness in TNWs/TNAs and TNAs to were decided by the anodizing condition. Figures 4.11(a1)-(d1) illustrate the working layer morphology and thickness and Figures 4.12(a2)-(d2) show the thickness of the films for DSSC application. The inner diameter and wall thickness of 30 V TNAs are 60 nm and 11 nm. The geometry of 40 V TNAs, the inner diameter is 70 nm and wall thickness is 10nm. The inner diameter of the 30V TNWs/TNAs is 60 nm, and 40 V TNWs/TNAs is 70 nm. Both bi-layer structures have the similar wall thickness 8-9 nm. Every sample has the same area of 0.28 cm^2 for fabricating DSSCs.

4.2.2 Measurement of dye adsorption amount

The enhanced DSSC performance may be attributed several factors such as increased dye adsorption amount, reduced recombination, and others.

In this study, all dye adsorption amount in different TiO_2 films were measured through the desorbed dye solution using UV-visible spectrum if calibrated. From the spectrum data, the dye adsorption of a TiO_2 film could be calculated by comparing the light absorption intensity of dye-desorbed NaOH solution. Beer-Lambert law, as expressed by Eqs.(4.1) and (4.2).

$$T = \frac{I}{I_0} = 10^{-\alpha * l} = 10^{-\varepsilon * c * l} \qquad (4.1)$$

$$A = -\log\left(\frac{I}{I_0}\right) = \varepsilon c l \qquad (4.2)$$

Where T is light transmittance, I is the absorption intensity, α is the absorption coefficient, l is the sample thickness, c is the concentration, ε is the extinction coefficient, and A is the light absorption. The absorbance at 505 nm wavelength of a solution with dye concentration 5×10^{-5} M is used as a reference. Thereby, the concentration can be calculated by using Eqs.(4.1) and (4.2), for a TiO_2 film thickness of 12 μm. Figure 4.13 shows the UV-visible spectra of the dye desorbed to NaOH solution for TNAs, TNWs/TNAs, and TiO_2 nanoparticle (TNPs) film. The dye adsorption of various TiO_2 films and its percentage relative to TiO_2 nanopaticle film are summarized in Table 4.1. TNWs/TNAs hybrid structure has a higher adsorption than TNAs due to the additional area from nanowires. Based on the absorption results, we know the TNWs/TNAs have a higher dye adsorption or surface area than TNAs only film. Therefore, we assume the more photons can be caught without escaping and inducing more initial current.

4.2-3 Cell Efficiency

The TiO_2 electrodes with different pore morphologies were fabricated into DSSCs, whose active area was 0.28 cm^2. The DSSC cell efficiency was characterized by scanning DSSC from -0.05V to 0.8V (with 0.01V per step) under AM1.5, 1 sun ($100mW/cm^2$) solar simulator illumination, which is typically described as I-V curve. The fill factor (FF) and cell overall energy conversion efficiency (η) were calculated from I-V curve by Eq.4-3 and Eq.4-4, which have been described in Chapter 2 in details.

$$FF = \frac{P_{MAX}}{V_{OC} \times I_{SC}} \tag{4-3}$$

$$\eta_{eff} = \frac{P_{MAX}}{P_{ill}} \times 100\% = \frac{V_{OC} \times I_{SC} \times FF}{P_{ill}} \times 100\% \tag{4-4}$$

Form this definition, we can see that the cell conversion efficiency affects by short circuit current density (J_{SC}), open circuit voltage (V_{OC}), and fill factor (FF). FF is an efficiency factor, used for checking whether the P_{MAX} is ideally equal to $V_{OC} \times I_{SC}$ or not. Open circuit voltage mainly affects by the TiO_2 material property, such as energy band gap and crystalline phase.

4.2.4 I-V characteristics

The I-V results of liquid electrolyte-based DSSCs using TNAs, TNWs/TNAs, and TiO_2 nanoparticle film as the photoelectrode, under AM 1.5, 1 Sun ($100mW/cm^2$) solar simulator illumination are summarized in Table 4.2. The Voc of various TiO_2 morphologies were about the same in the range of 0.61-0.63V, which was determined by the number of electrons stored in TiO_2, which in turn was set by the recombination of thermalized electrons in the nanostructure.

For TNWs/TNAs and TNA prepared under 40 V (at the same total thickness of 12 μm), J_{sc} increased from 3.71 to 5.08 mA/cm^2, while the conversion efficiency was raised from 0.81% to 1.57% for TNA and TNWs/TNAs, respectively. When a lower anodizing voltage, 30 V was used, the tube inner diameter was reduced to ~60 nm from 70 nm prepared under 40V. This led to an improved of J_{SC} and conversion efficiency as observed for TNAs (3.81 mA/cm^2 and η=1.08) and TNWs/TNAs (5.27 mA/cm^2 and η=1.85). Such enhancement can be attributed to the increased dye adsorption amount and better electron transport in TNWs/TNAs compared to TNAs only. When the thickness of TNAs/TNWs was raised to 15 μm, J_{sc} and conversion efficiency were increased to 6.84 mA/cm^2 and 2.02.%, respectively.

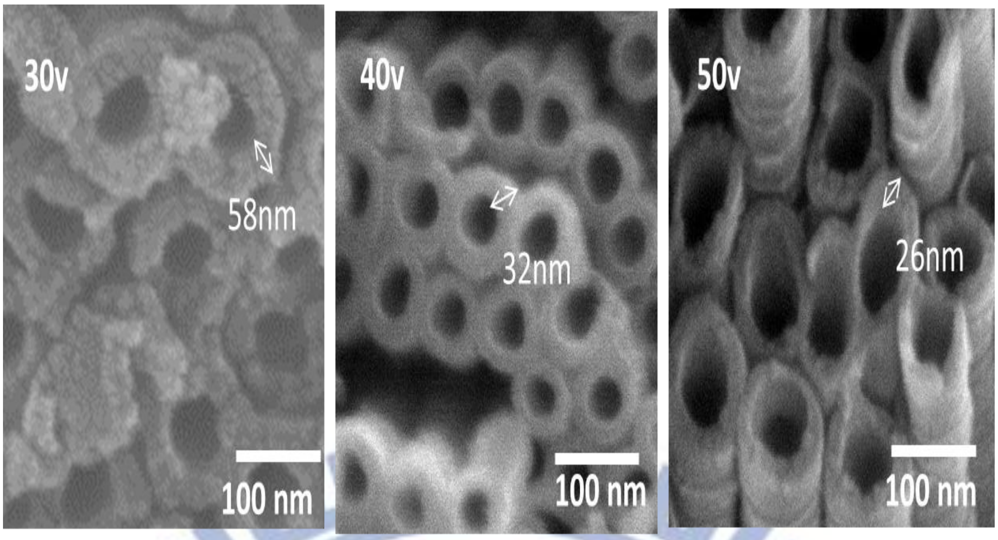

Figure 4.1 SEM images of TiO_2 films prepared by various anodizing voltage: (a)30 V, (b) 40 V, and (c) 50 V for 0.5h.

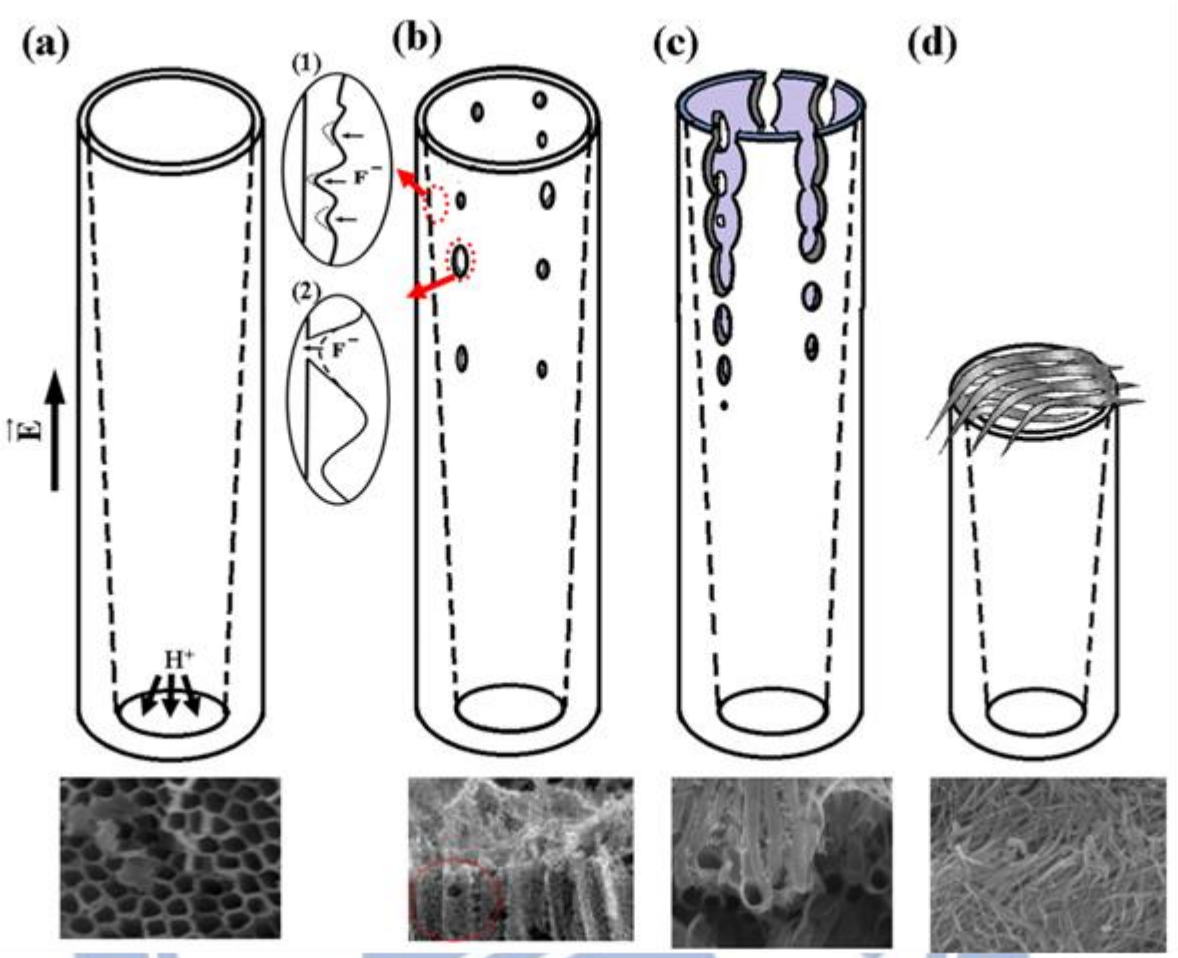

Figure 4.2 Schematic diagrams along with their corresponding surface morphology SEM images for four key stages in the TNWs/TNAs formation mechanism: (a) thinning the tube wall thickness with high roughness near the TNAs mouths, (b) forming strings of through holes in the top section of TNAs, (c) splitting into nanowires, and (d) collapsing and further thinning of nanowires [100].

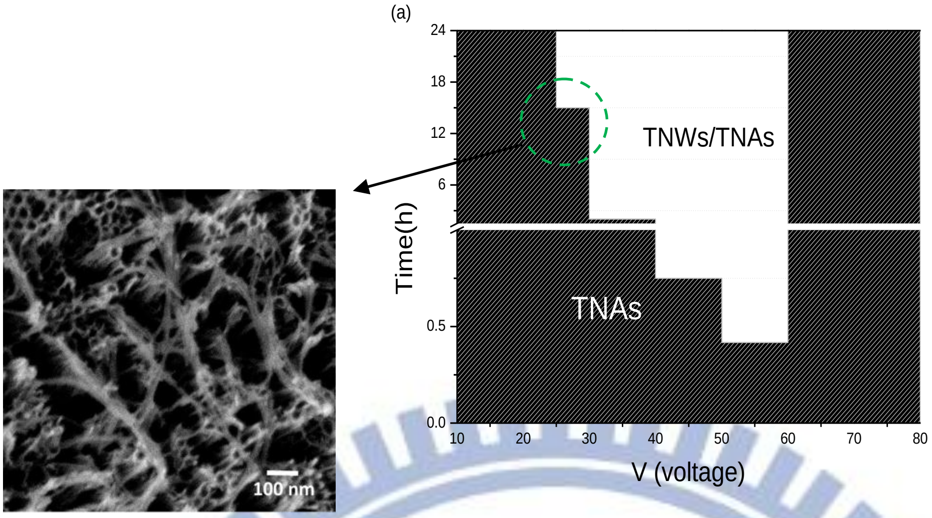

Figure 4.3 The condition of required anodizing voltage and processing time (shaded zone) for forming forming TNWs/TNAs (white zone) and the excluded shaded zone for forming TNAs only.

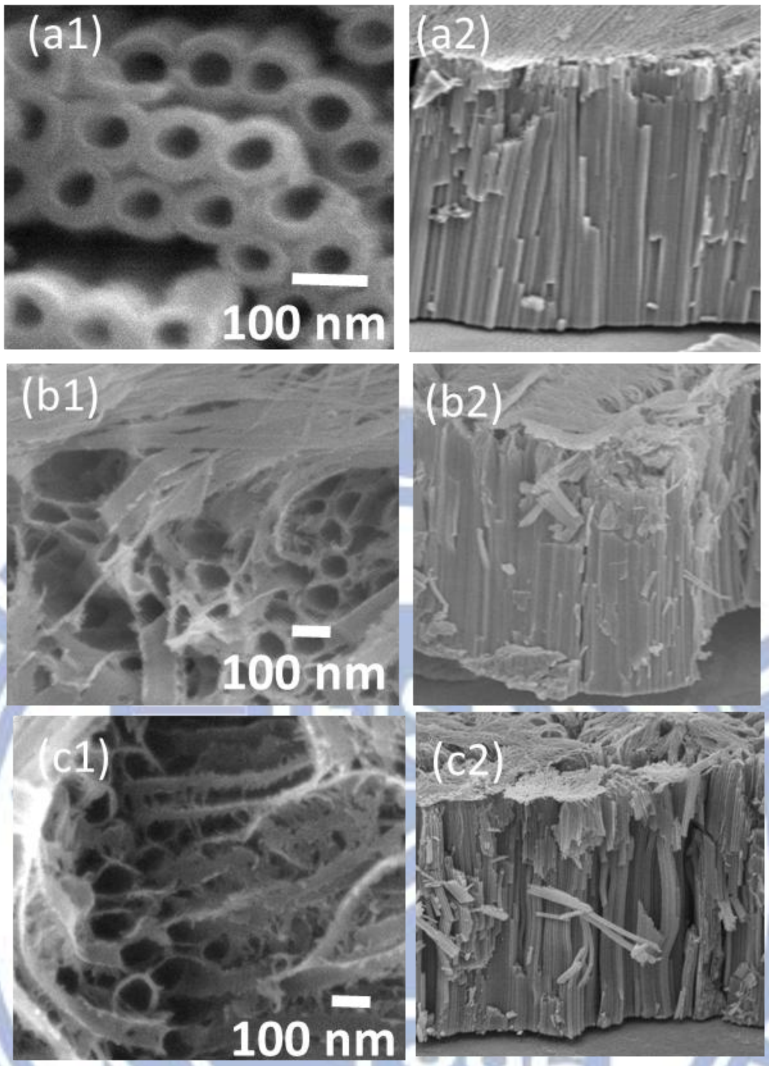

Figure 4.4 (1) Surface and (2) cross-sectional morphology of TNWs/TNAs hybrid structure under anodizing voltage of 40 V and various anodization time: (a) 0.5h, (b) 2h , and (c) 4h.

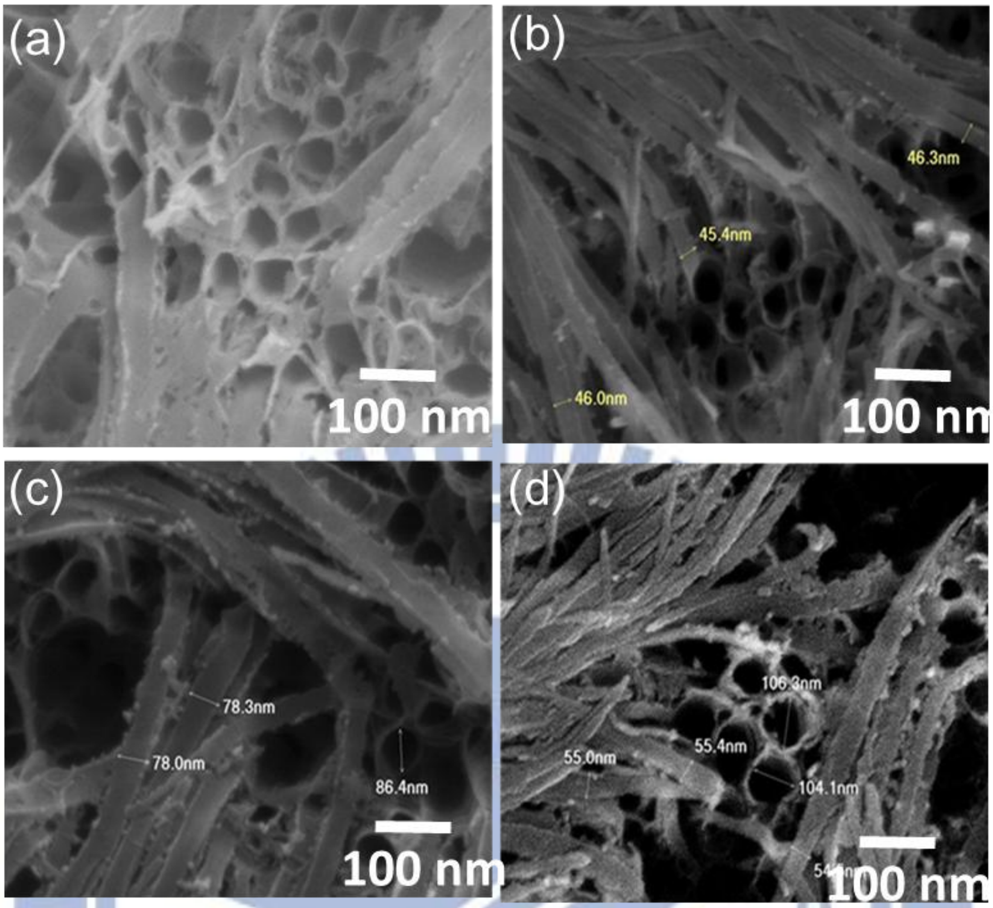

Figure 4.5 Surface morphology of TNWs/TNAs hybrid structure near the tube mouth films prepared at 40 V and under different anodizing time: (a) 2 h, (b) 3 h, (c) 4 h, and (d) 5 h.

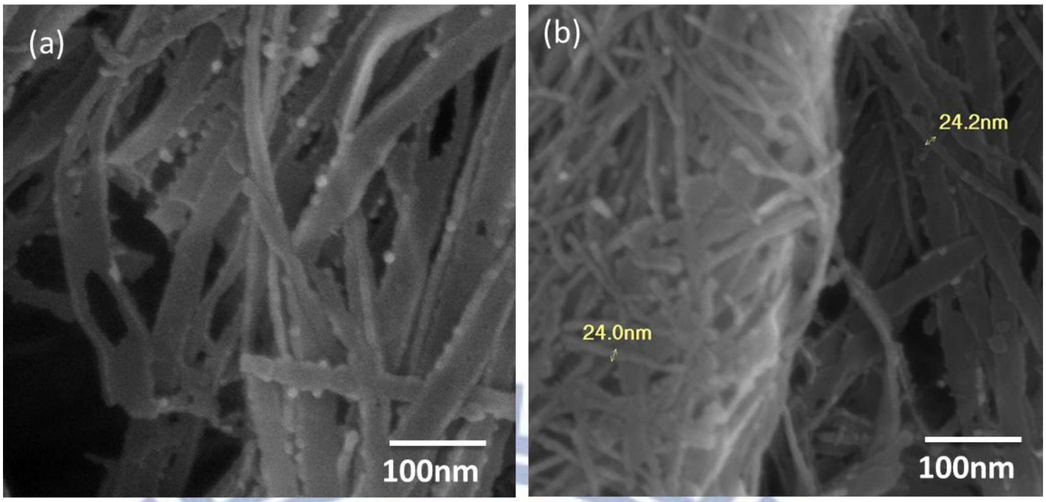

Figure 4.6 Surface morphology from nanobelts to nanowires under 40 V for 4 h: (a) holes on the nanobelt, and (b) nanowires with smaller width.

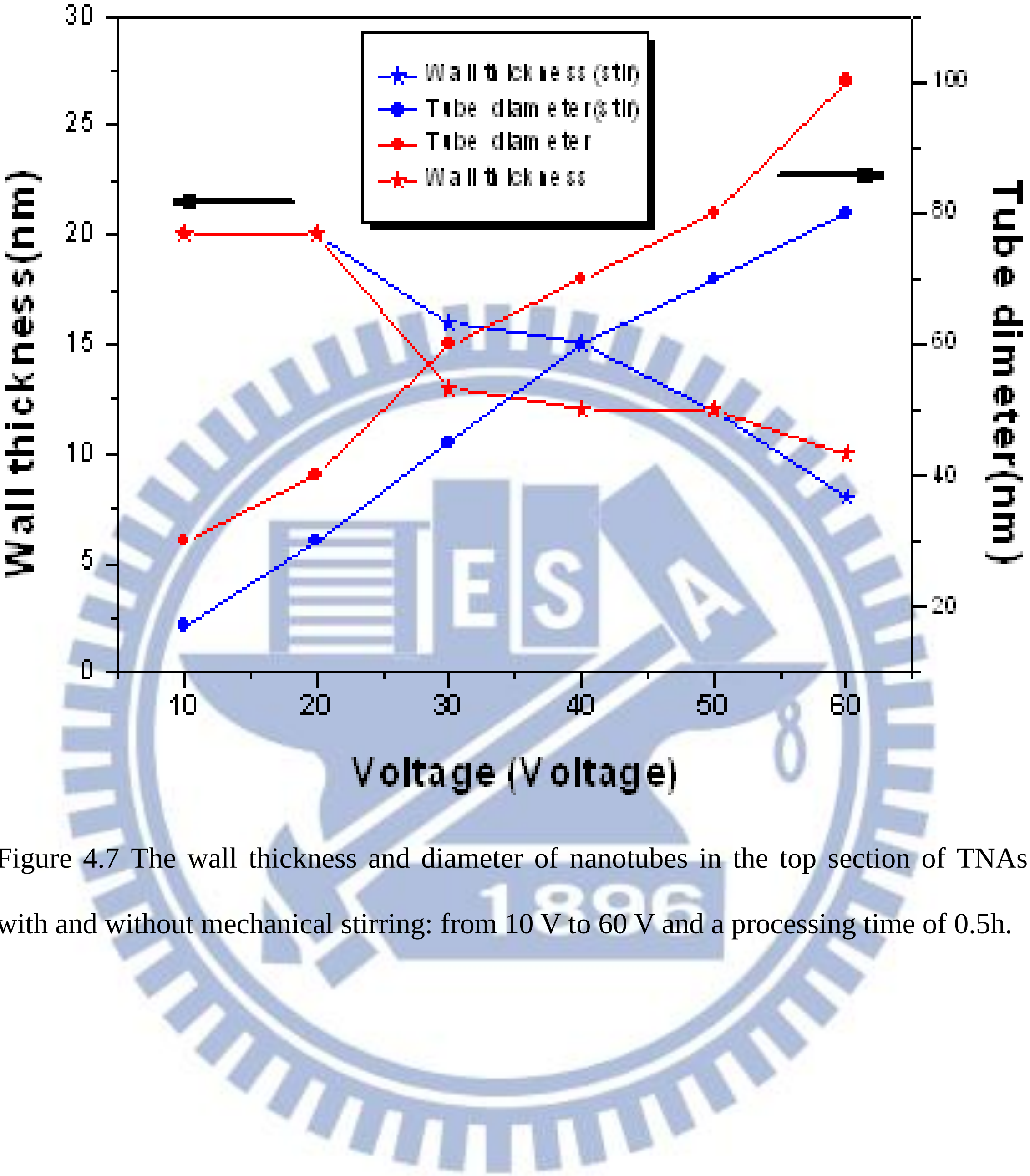

Figure 4.7 The wall thickness and diameter of nanotubes in the top section of TNAs with and without mechanical stirring: from 10 V to 60 V and a processing time of 0.5h.

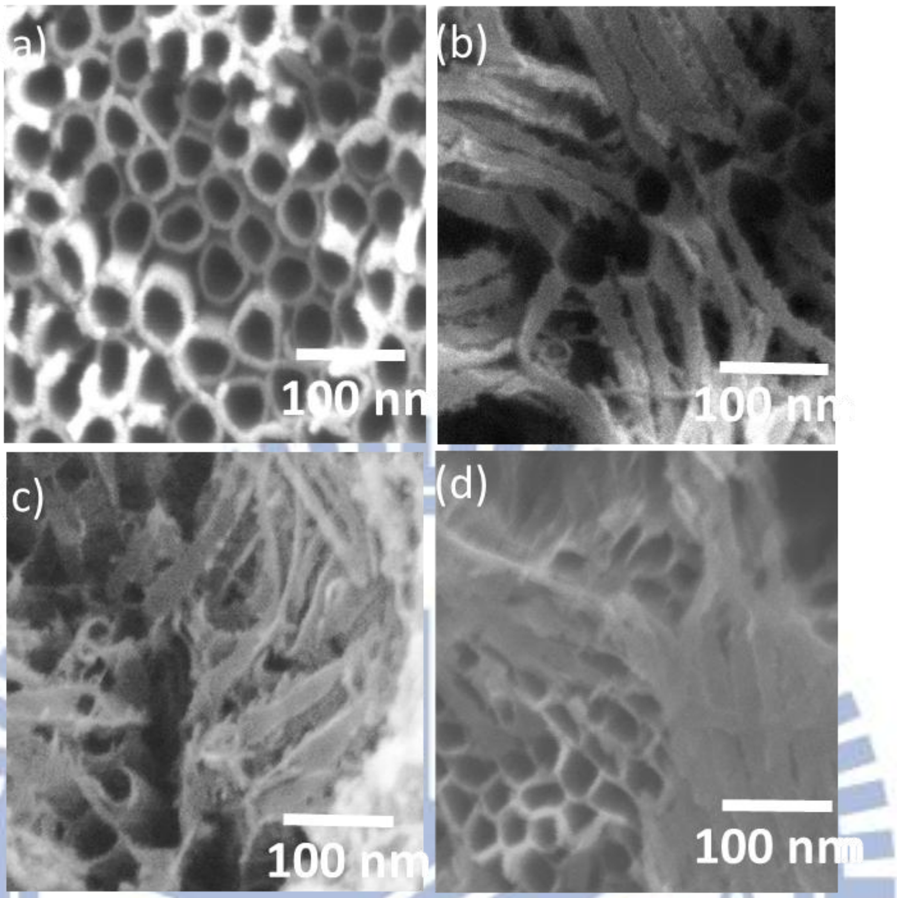

Figure 4.8 SEM images of the TiO_2 films prepared by anodic oxidation for 30 V under different conditions: (a) mechanical stirring for 4 h, (b) mechanical stirring for 6 h, (c) non-stirring for 4 h, and (d) non-stirring for 6 h.

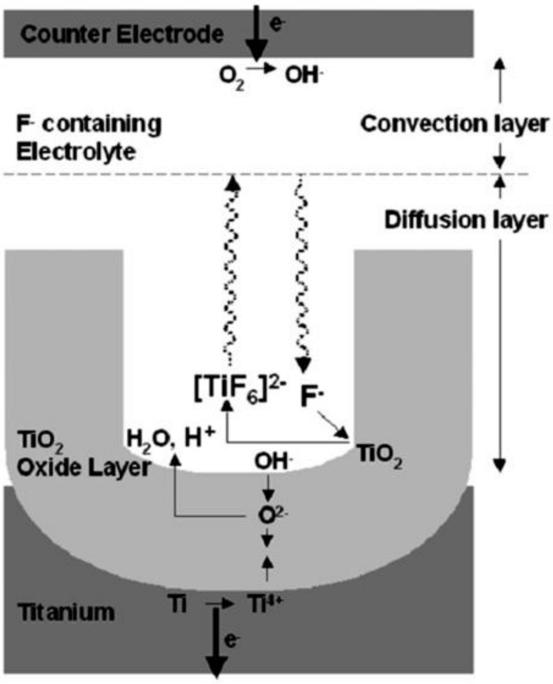

Figure 4.9 Schematic representations of relevant processes in TiO_2 nanotube formation and dissolution. [104]

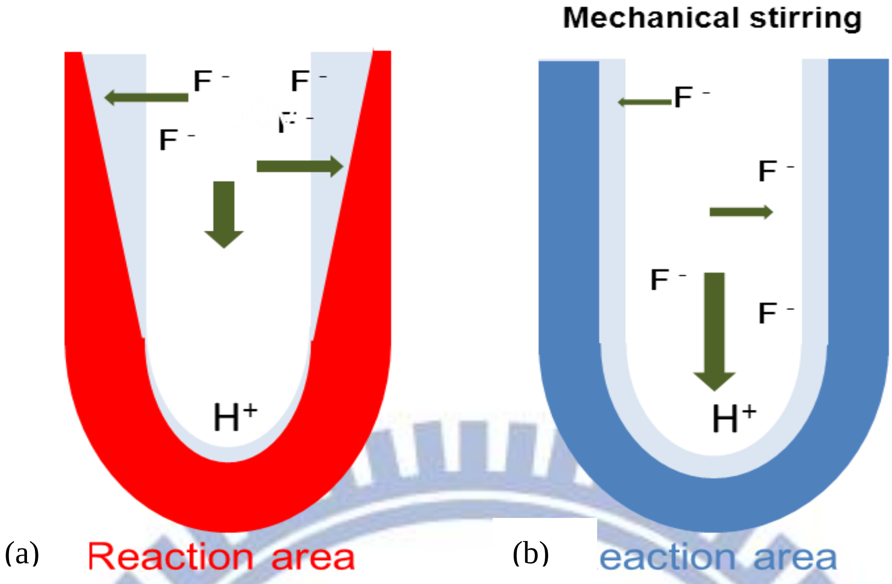

Figure 4.10 Schematic diagrams along with the consideration of the transport processes of ionic species (F$^-$, O^{2+}, and H$^+$) : (a) non-stirring, and (b) stirring.[81]

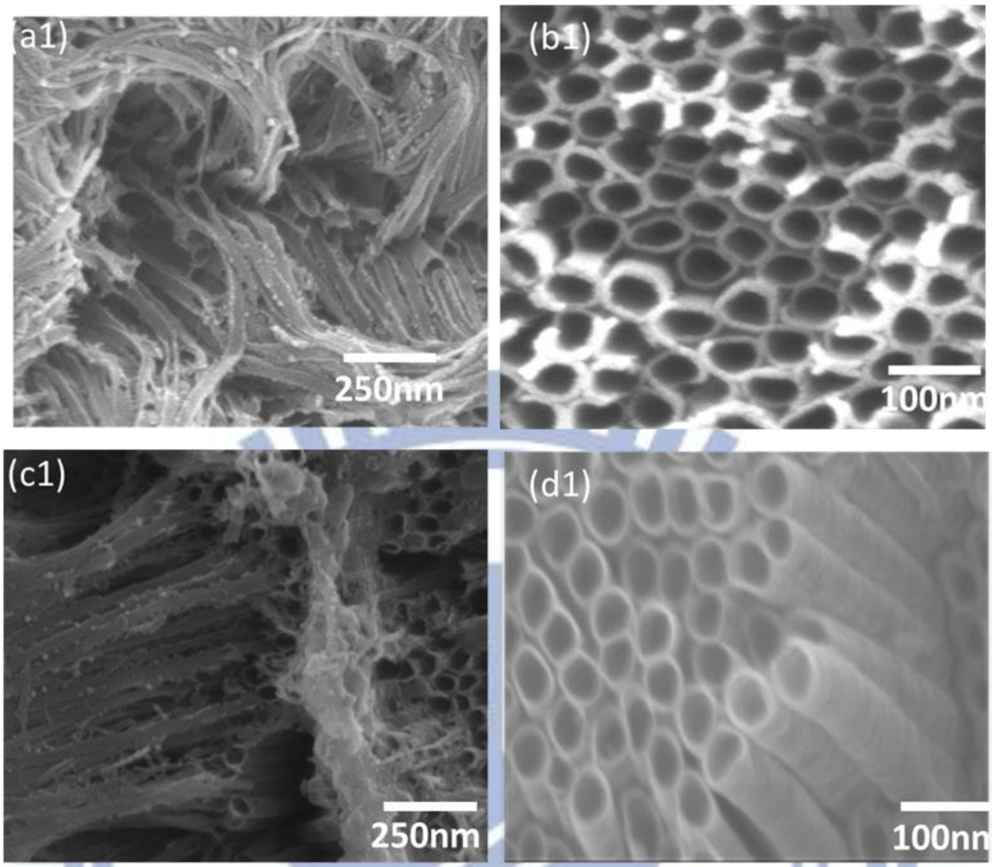

Figure 4.11 SEM images of TiO_2 films used in DSSCs: (a1) 40 V/TNWs/TNAs, (b1) 30V TNA, (c1) 30V/TNWs/TNAs, and (d1) 40V/TNA

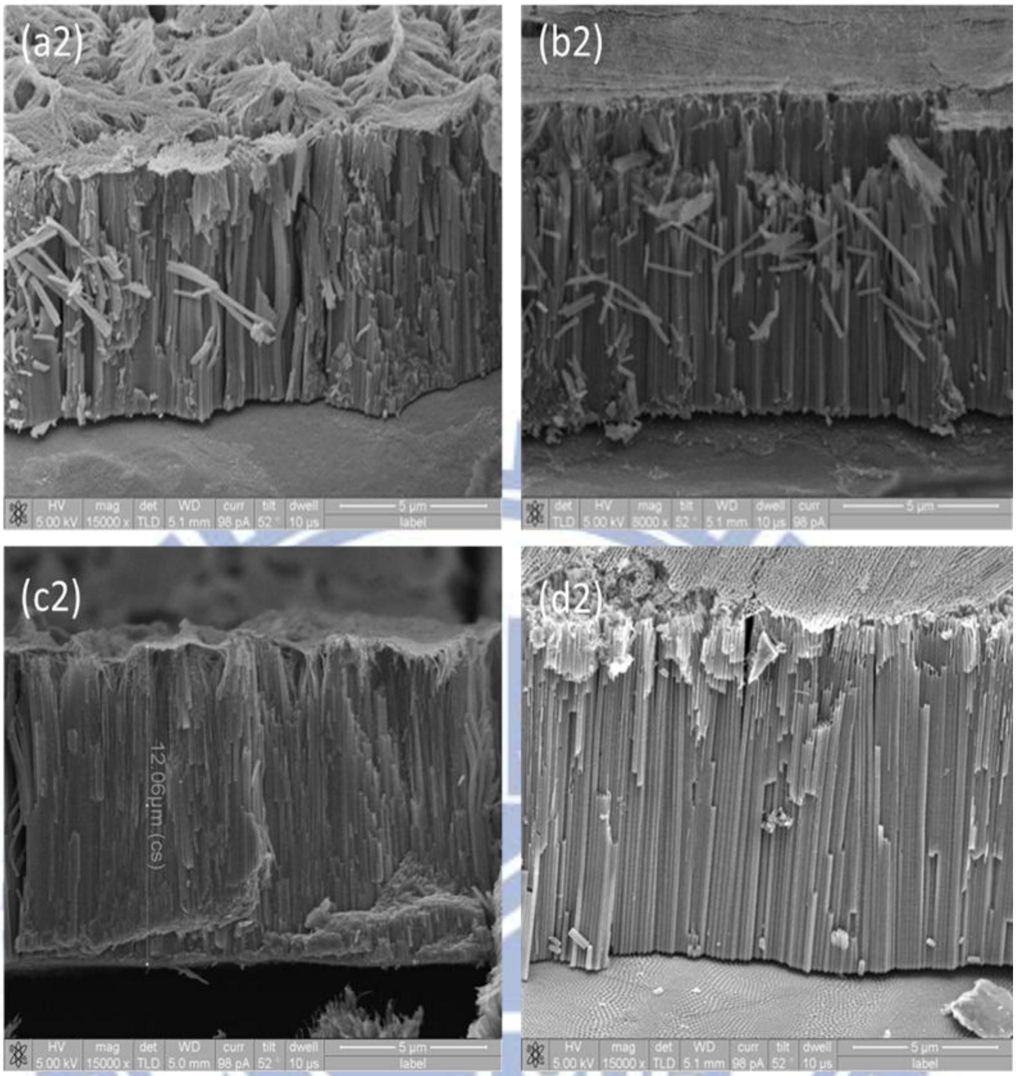

Figure 4.12 SEM images of thickness TiO$_2$ films used in DSSCs: (a2) 40V/TNWs/TNAs, (b2) 30V TNAs, (c2) 30V/TNWs/TNAs, and (d2) 40V/TNAs

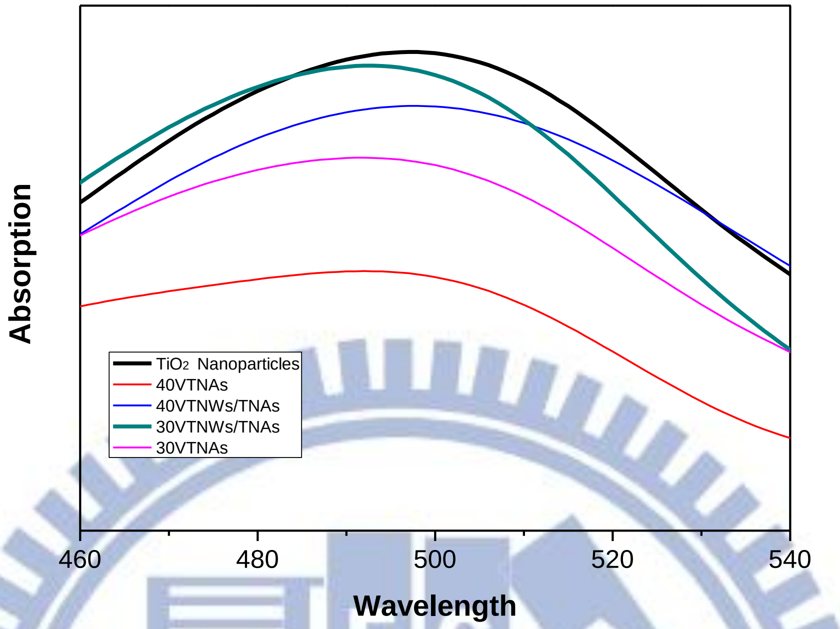

Figure 4.13 UV-Visible spectra of the desorbed dye from the solutions of various TNAs, TNA/TNWs, and TiO_2 nanoparticles films.

Table 4.1 Dye adsorption of various TiO_2 films and its percentage relative to TiO_2 nanopaticle film

TiO_2 film	Dye adsorption($\times 10^{-6}$) mol/cm^2	Change relative to nanoparticles film (%)
30V TNWs/TNAs	4.53	86
40V TNWs/TNAs	4.36	83
30V TNAs	3.00	65
40V TNAs	2.60	47
TiO_2 Nanoparticles film	5.29	100

Table 4.2 I-V relationship of liquid electrolyte-based DSSCs using TNAs, TNWs/TNAs, and TiO_2 nanoparticle film as the photoelectrode

Sample	30V TNAs (12µm)	30V TNWs/TNAs (12µm)	40V TNAs (12µm)	40V TNWs/TNAs (12µm)	40V TNWs/TNAs (15µm)
Voc (V)	0.61	0.63	0.61	0.64	0.63
Jsc(mA/cm^2)	3.81	5.27	3.71	5.08	6.87
FF	0.45	0.56	0.42	0.48	0.47
η (%)	1.04	1.85	0.81	1.57	2.02

Chapter 5 Conclusion

This study investigates a one-step method for the fabrication of a TNWs-covered TNAs (TNWs/TNAs) hybrid structure, using a mixture of EG and water containing NH_4F electrolyte with and without mechanical stirring. The morphology of the TNWs/TNAs structure was then examined by changing the anodizing voltage and processing time, to elucidate the detailed formation mechanism of TNWs/TNAs.

In specific, various TNAs and TNWs/TNAs structure can be fabricated by using anodizing voltage from 25 to 60 V for various processing time. In addition, we add a stirring bar to rotate the electrolyte during the anodizing experiment. This increases the TNA tube length but postpones the emergence of nanowire. Through the control of anodizing voltage, processing time, and mechanical stirring, the thickness of TNAs and TNWs/TNAs structure are kept the same at 12 mm, while the tube diameter and wall thickness are varied according to the processing conditions.

The DSSC performance of TNWs/TNAs and TNAs structures was then investigated and compared with the film made of TiO_2 nanoparticles using a DSSC area size of 0.28cm^2. For TNWs/TNAs hybrid structure (30V, 8 hours), the conversion efficiency and J_{sc} are 1.85%, 5.27 mA/cm^2, compared to 1.04% and 3.81 mA/cm^2 in a TNA only film. The 44.3% improvement in conversion efficiency can be attributed to the enhanced dye adsorption (21%) and mass transport in TNWs/TNAs compared to TNAs only. Moreover, the conversion efficiencies in TNWs/TNAs and TNAs only films fabricated under 40 V are lower than those under 30 V due to lower surface area originated from larger inner diameter, as evidenced by dye adsorption amount. When the length up to 15 µm, the efficiency (η%) is further increased to 2.02%. Although the efficiency of TNWs/TNAs film is still lower than that of TiO_2 nanoparticle film, TNWs/TNAs films provide a simple and efficient method to be a flexible DSSC.

Future Work

There are plenty of opportunities to improve the performance in the DSSC based on TNWs/TNAs hybrid structure. Several approaches are recommended below for future work:

Methods for enhancing the dye adsorption amount to induce higher photocurrent

(a) To enhance the surface area through smaller tube diameter and larger surface roughness

  (1) We can use different anodizing voltage to fabricate the different inner diameter nanotube array and expecting for a better dye adsorption.

  (2) The surface area of TNWs/TNAs hybrid structure can be enhanced by increasing its surface roughness. This can be achieved by using a two-step process: (1) first, to carry out the anodizing process with a stirring bar to obtain a more homogeneous and collapsed TNWs. And then (2) After the formation of nanowire using stirring method, the stirring can to shut down to enhance the etch rate in the top section of TNAs and nanorwires. (3) to apply different rate of rotation and/or a periodic variation voltage to deliver various roughness inside the nanotubes. [80]

(b) To improve the adsorption of dye onto TNWs/TNAs hybrid structure.

Currently, vacancies are still observed after the dye has been immersed in to hybrid structure for 48 hours. Therefore, it may be useful to add a coadsorbent into DSSCs system which can serve as a buffer blocking water and triiodide from the surface of TiO_2. Diphenylphosphinic acid (DPPA) is one of the coadsorbent candidate [105]

(c) To improve the electrolytes

One can change the source of I ions, or modify the concentration of electrolyte for providing electrons to redox the oxidized dye molecules. [106,107]

References

---

1. M. Grätzel, Nature **414**, 338 (2001)

2. B. O'Regan and M. Grätzel, Nature **353**, 737 (1991)

3. A. Yella, H.-W. Lee, H. N. Tsao, C. Yi, A. K. Chandiran, M. K. Nazeeruddin, E. W.-G. Diau, C.-Y. Yeh, S. M. Zakeeruddin and M. Grätzel, Science, **334** ,629 (2011).

4. I. Turkevych, Y. Pihosh, K. Hara, Z. S. Wang, and M. Kondo Jpn. J. Appl. Phys. **48**, 06FE02 (2009)

5. G. K. Mor, O. K. Varghese, M. Paulose, K. Shankar, and C. A. Grimes, Sol. Energy Mater. Sol. Cells, **90**, 2011 (2006)

6. L. Zhao, J. Yu, J. Fan, P. Zhai, and S. Wang, Electrochem. Commun., **11**, 2052 (2009)

7. K.-M. Lee,V. Suryanarayanan, J.-H. Huang, K. R. J. Thomas, J. T. Lin, and K.-C. Ho, Electrochim. Acta, **54**, 4123 (2009)

8. Y. Alivov and Z. Y. Fan, Appl. Phys. Lett., **95**, 0635504 (2009)

9. M.R. Hoffmann, S.T. Martin, W. Choi, and D.W. Bahnemann, Chem. Rev., **95**, 69 (1998)

10. J. H. Lim and J. Choi, Small, **3**,1504 (2007)

11. Tomas Markvart, <u>Solar Electricity</u>, John Wiley & Sons, LTD., New York,(1994), pp. 5-19.

12. M. Grätzel, Curr. Opin. Colloid Interface Sci., **4**, 314 (1999)

13. Z. S. Wang, H. Kawauchi, T. Kashima, and H. Arakawa, Coordination Chemistry Reviews, **248**, 1381 (2004)

14. M. Grätzel, J. Photochem. Photobiol. A, **164**, 3 (2004)

15. D. Cahen, G. Hodes, M. Grätzel, J. F. Guilemoles, and I. Riess, J. Phys. Chem. B **104**, 2053 (2000)

16. C. J. Barbe, F. Arendse, P. Comte, M. Jirousek, F. Lenzmann, V. Shklover, and M.

Grätzel, J. Am. Ceram. Soc., **80**, 3157 (1997)

17. K. Kalyanasundaram and M. Grätzel, Coord. Chem. Rev., **177,** 347 (1998)
18. D.S. Tsoukleris, I. M. Arabatzis, E. Chatzivasiloglou, A. I. Kontos, V. Belessi, M. C. Bernard, and P. Flaras, Sol. Energy, **79**, 422 (2005)
19. S. Karuppuchamy, K. Nonomura, T. Yoshida, T. Sugiura, and H. Minoura, Solid State Ion., **151**, 19 (2002)
20. S. Karuppuchamy, D. P. Amalnerkar, K. Yamaguchi, T. Yoshida, T. Sugiura, and H. Minoura, Chem. Lett., **1**,78 (2001)
21. M. S. Wong, T. S. Yang, and C. B. Shiu, Surf. Sci. **548**, 75 (2004)
22. S. B. Amor, G. Baud, J. P. Besse, and M. Jacquet, Thin Solid Films **293**, 163 (1997)
23. M. Gomez, E. Magnusson, E. Olsson, A. Hagfeldt, S. E. Lindquist, and C. G. Granquiat, Sol. Energy Mater. Sol. Cells, **62**, 269 (2000)
24. D. Dumitriu, Appl. Catal. B-Environ., **25**, 83 (2000)
25. K. Okimura, Surf. Coat. Technol., **135**, 186 (2001)
26. P. Zeman and S. Takabayashi, Surf. Coat. Technol., **153**, 93 (2002)
27. D. Byun, J. Hazard. Mater., **73**, 199 (2000)
28. D. R. Burgess, P. A. Morris, T. J. Anderson, and J. L. Hohman, J. Cryst. Growth, **166**, 763 (1999)
29. M. Paulose, K. Shankar, O. K. Varghese, G. K. Mor, and C. A. Grimes, J. Phys. D: Appl. Phys., **39**, 2498 (2006)
30. B. Tan and Y. Y. Wu, J. Phys. Chem. B, **110**, 15932 (2006)
31. J. M. Macak, H. Tsuchiya, L. Taveira, and P. Schmuki, Angew. Chem. Int. Ed.,**44**, 100(2005)
32. J. M. Macak, H. Tsuchiya, L. Taveira, S. Aldabergerova, and P. Schmuki, Angew. Chem. Int. Chem. Int. Ed., **44**, 463(2005)
33. T. Naoki and Y. Wang, Langmuir, **10**, 4574 (1994)
34. S. R. Brankovic, J. McBreen, and R. R. Adzic, Surf. Sci., **479**, L363 (2001)

35. A. Kay and M. Grätzel, Sol. Energy Mater. Sol. Cells, **44,** 99 (1996)

36. S. Cherian and C. C. Wamser, J. Phys. Chem. B, **104**, 3624 (2000)

37. H. L. Hsu, W. T. Hsu, and J. Leu, Electrochimi. Acta, **56**, 5904 (2011)

38. J. Hagen, W. Schaffrath, P. Otschik, R. Fink, A. Bacher, H. W. Schmidt, and D. Haarer, Synth. Met., **89**, 215 (1997)

39. Y. X. Li, J. Hagen, W. Schaffrath, P. Otschik, and D. Haarer, Sol. Energy Mater. Sol. Cells, **56**, 167 (1999)

40. M. Okuya, K. Nakade, and S. Kaneko, Sol. Energy Mater. Sol. Cells, **70**, 425 (2002)

41. T. L. Ma, K. Inoue, H. Noma, K. Yao, and E. Abe, J. Photochem. Photobiol. A-Chem., **152**, 207 (2002)

42. G. Namutdinova, S. Sensfuss, M. Schrodner, A. Hinsch, R. Sastrawan, D. Gerhard, S. Himmler, and P. Wasserscheid, Solid State Ion., **177**, 3141 (2006)

43. P. Wang, S. M. Zakeeruddin, J. E. Moser, M. K. Nazeeruddin, T. Sekiguchi, and M. Grätzel, Nature Mate., **2**, 498 (2003)

44. W. Kubo, S. Kambe, S. Nakade, T. Kitamura, K. Hanabusa, Y. Wada, and S. Yanagida, J. Phys. Chem. B, **107**, 4374 (2003)

45. H. Usui, H. Matsui, N. Tanabe, and S. Yanagida, J. Photochem. Photobiol. A-Chem., **164**, 97 (2004)

46. S. Yanagida, M. Watanabe, H. Matsui, K. Okada, H. Usui, T. Ezure, and N. Tanabe, Fujikura Techn. Rev., **34**, 59 (2005)

47. W. Kubo, K. Murakoshi, T. Kitamura, S. Yoshida, M. Haruki, K. Hanabusa, H. Shirai, Y. Wada, and S. Yanagida, J. Phys. Chem. B, **105**, 12809 (2001)

48. R. Kawano, H. Matsui, C. Matsuyama, A. Sato, M. Susan, N. Tanabe, and M. Watanabe, J. Photochem. Photobiol. A-Chem., **164**, 87 (2004)

49. S. S. Kim, K. W. Park, J. H. Yum, and Y. E. Sung, J. Photochem. Photobiol. A-Chem., **189**, 301 (2007)

50. S. S. Kim, K. W. Park, J. H. Yum, and Y. E. Sung, Sol. Energy Mater. Sol. Cells, **90**, 283 (2006)

51. X. M. Fang, T. L. Ma, G. Q. Guan, M. Akiyama, and E. Abe, J. Photochem. Photobiol. A-Chem., **164**, 179 (2004)

52. S.-S. Kim, K.-W. Park, J.-H. Yum, Y.-E. Journal of Photochemistry and Photobiology A: Chemistry **189**, 301 (2007)

53. N. Papageorgiou, Coord. Chem. Rev., **248**, 1421 (2004)

54. Y. Chiba, A. Islam, Y. Watanabe, R. Komiya, N. Koide, and L. Y. Han, Japanese J. Appl. Phys. Part 2-Letters & Express Letters, **45**, L638 (2006)

55. T. C. Wei, C. C. Wan, and Y. Y. Wang, J. Phys. Chem. C, **111**, 4847 (2007)

56. T. C. Wei, C. C. Wan, and Y. Y. Wang, Appl. Phys. Lett., **88**, 103122 (2006)

57. Y. Saito, W. Kubo, T. Kitamura, Y. Wada, and S. Yanagida, J. Photochem. Photobiol. A-Chem., **164**, 153 (2004)

58. Y. Saito, T. Kitamura, Y. Wada, and S. Yanagida, Chem. Lett., **31**, 1060 (2002)

59. E. Ramasamy, W. J. Lee, D. Y. Lee, and J. S. Song, Appl. Phys. Lett., **90**, 173103 (2007)

60. K. Imoto, K. Takahashi, T. Yamaguchi, T. Komura, J. Nakamura, and K. Murata, Sol. Energy Mater. Sol. Cells, **79**, 459 (2003)

61. R. Kikuchi, T. Hoshikawa, and K. Eguchi, J. Electroanal. Chem., **588**, 59 (2006)

62. K. Suzuki, M. Yamaguchi, M. Kumagai, and S. Yanagida, Chem. Lett., **32**, 28 (2003)

63. T. Kitamura, M. Maitani, M. Matsuda, Y. Wada, and S. Yanagida, Chem. Lett., **10**,1054 (2001)

64. N. Ikeda, K. Teshima and T. Miyasaka, Chem. Commun., 1733-1735 (2006)

65. S. Ito, N. L. C. Ha, G. Rothenberger, P. Liska, P. Comte, S. M. Zakeeruddin, P. Pechy, M. K. Nazeeruddin, and M. Grätzel, Chem. Commun., **38**, 4004 (2006)

66. P. M. Sommeling, B. C. O'Regan, R. R. Haswell, H. J. P. Smit, N. J. Bakker, J. J. T. Smits, J. M. Kroon, and J. A. M. van Roosmalen, J. Phys. Chem. B, **110**, 19191 (2006)

67. C. J. Barbe, F. Arendse, P. Comte, M. Jirousek, F. Lenzmann, V. Shklover, and M.

Grätzel, J. Am. Ceram. Soc., **80**, 3157 (1997)

68. M. K. Nazeeruddin, A. Kay, I. Rodicio, R. Humphrybaker, E. Muller, P. Liaka, N. Vlachopoulos, and M. Grätzel, J. Am. Ceram. Soc., **115**, 6382 (1993)
69. N. G. Park, G. Schlichthorl, J. van de Lagemaat, H. M. Cheong, A. Mascarenhas, and A. J. Frank, J. Phys. Chem. B, **103**, 3308 (1999)
70. P. M. Sommeling, B. C. O'Regan, R. R. Haswell, H. J. P. Smit, N. J. Bakker, J. J. T. Smits, J. M. Kroon, and J. A. M. van Roosmalen, J. Phys. Chem. B, **110**, 19191 (2006)
71. S. Ito, P. Liska, P. Comte, R. L. Charvet, P. Pechy, U. Bach, L. Schmidt-Mende, S. M. Zakeeruddin, A. Kay, M. K. Nazeeruddin, and M. Grätzel, Chem. Commun., **41**, 4351 (2005)
72. S. Hore and R. Kern, Appl. Phys. Lett., **87**, 263504 (2005)
73. V. Zwilling, E.D. Ceretti, A.B. Forveille, D.David, M. Y. Perrin, and M. Aucouturier, Surf. Interface Anal., **27**, 629 (1999)
74. J. M. Macak, K. Sirotna, and P. Schmuki, Electrochim. Acta, **50**, 3679 (2005)
75. Q. Cai, M. Paulose, O.K. Varghese, and C. A. Grimes, J. Mater.Res., **20**, 230 (2005)
76. G. K. Mor, K. Shankar, M. Paulose, O. K. Varghese, C. A. Grimes, Nano Lett. **5**,191. (2005)
77. J.M. Macak, H. Tsuchiya, L. Taveria, S. Aldabergerova, and P. Schmuki, Angew. Chem. Int. Ed., **44**, 7463 (2005)
78. M. Paulose, K. Shankar, S. Yoriya, H.E. Prakasam, O.K. Varhese, G.K. Mor, T. J. Latempa, A. Fitzgerald, and C. A. Grimes, J. Phys. Chem. B, **110**, 16179 (2006)
79. H.E. Parkasam, K. Shankar, M.Paulose, O.K. Varghese, and C. A. Grimes, J. Phys. Chem. C, **111**,7235 (2007)
80. K. Shakar, G. K. Mor, H. E. Prakasam, S. Yoriya, M. Paulose, O. K. Varghese and C. A. Grimes, Nanotechnology, **18**, 065707 (2007)
81. G.E. Thomson, Thin Solid Film, **297,** 192 (1997)

82. H. Liu, Tao, and W. Shen, Nanotechnology, **22**,155603(2011)

83. G. K. Mor, K. Shankar, M. Paulose, O. K. Varghese, and C. A. Grimes, Nano.Lett. **5**, 191 (2005)

84. K. Zhu, N.R. Neale, A. Miedaner, and A. J. Frank, Nano Lett., **7,** 69 (2007)

85. T. Stergiopoulos, A. Ghicov, V. Likodimos, D.S. Tsoukleris, J. Kunze, P. Schmuki, and P. Falaras, Nanotechnology, **19**, 235602 (2008)

86. J. R. Jennongs, A. Ghicov, L. M. Peter, P. Schmuki, and A. B. Walker, J. Am. Chem. Soc., **130**, 13364 (2008)

87. D. J. Yang, H. Park, S. J. Cho, H. G. Kim, and W. Y. Choi, J. Phys. Chem. Solids, **69**, 1272 (2008)

88. C. J. Barbe, F. Arendse, P. Comte, M. Jirousek, F. Lenzmann, V. Shklover, and M. Grätzel, J. Am. Ceram. Soc., **80**, 3157 (1997)

89. K. Kalyanasundaram and M. Grätzel, Coord. Chem. Rev., 1**77,**347 (1998)

90. L. Zhao, J. Yu, J. Fan, P. Zhai, and S. Wang, Electrochem. Commun., **11**, 2052 (2009)

91. H. Yin, Y. Wada , T. Kitamura , S. Kambe , S. Murasawa , H. Mori, T. Sakata and S. Yanagida, Journal of Materials Chemistry **11**, 1694 (2001)

92. J. Wang, L. Zhao, Victor S. Y. Lin and Z. Q. Lin: J. Mater. Chem. **19**, 3682-3687 (2009)

93. H. Tao, J. Tao, T. Wang, and Z. Bao, Advanced Materials Research 463-464 (2012)

94. S.D. Mo., and W. Y. Ching, Phys. Rev. B, **51**, 13023 (1995)

95. Z.H. Zhou, W. K. Li and Z. Q. Chen, Key Eng Mater., **1462**, 368-372 (2008)

96. J. G. Li, T. Ishigaki, and X Sun, J. Phys. Rev. B **51**, 13023 (1995)

97. M. Grätzel, Prog. Photovolt. Res. Appl., **8**, 171 (2000)

98. M. Grätzel, Inorg. Chem., **44**, 6841 (2005)

99. K. Fan, M. Liu, T. Peng, L. Ma,K, Dai, Renewable Energy, 35, 555 (2010)

100. M.-Y. Hsu, "Morphological and Microstructural study on TiO2 nanotube arrays and hybrid structure and their photocatalytic performance", Ph.D. Dissertation, National Chiao Tung University (2012)

101. L. Sun, S. Zhang, X. W. Sun, and X. He, J. Electroanal. Chem.,**637**, .6 (2009).

102. H. Yin, H. Liu, and W. Z. Shen, Nanotechnology, **21** ,035601 (2010)

103. H. Liu, L. Tao, and W. Shen, Nanotechnology, **22**,155603 (2011)

104. D. Kim, F. Schmidt-Stein, R. Hahn and P. Schmuki Electrochem. Commun. **10**, 1082 (2008)

105. Lin, H.; Liu, Y.; Li, X.; Zhang, J.; Wang, N.; Li, J. *Electrochimica Acta* vol. 56 issue 5,2092-2097 (2011).

106. S.-H. Anna Lee, A.-M.S. Jackson, A. Hess, S.-T. Fei, S.M. Pursel, J. Basham, C.A. Grimes, M.W. Horn, H.R. Allcock, T.E. Mallouk, J. Phys. Chem. C **114**,15234-15242. (2010)

107. Yu, B.; Cao, Y.; Zhang, J.; Wang, M.; Li, R.; Wang, P.;Zakeeruddin, S. M.; Grätzel, M. Nature Mater., **7**, 626. (2008)